

UNCOLLIDED FLUX FROM FINITE
RIGHT-CIRCULAR CYLINDER
VIEWED ENDWISE

by

LARRY A. RASH

B. S., Kansas State University, 1957

A MASTER'S THESIS

submitted in partial fulfillment of the

requirements for the degree

MASTER OF SCIENCE

Department of Nuclear Engineering

KANSAS STATE UNIVERSITY
Manhattan, Kansas

1962

LD
2668
T4
1962
R37
C.2

Documents

TABLE OF CONTENTS

INTRODUCTION.....	1
NOMENCLATURE.....	2
THEORETICAL DEVELOPMENT.....	3
Problem.....	3
Solutions.....	5
Stacked Disk Solution.....	5
Large Cone Approximation.....	6
Small Cone Approximation.....	6
Equivalent Volume Cone Approximation.....	6
Equivalent Circular Plane Source Approximation.....	7
NUMERICAL ANALYSIS.....	8
Method of Solution.....	8
Preliminary Investigations.....	8
Accuracy Analysis of Stacked Disk Solution.....	8
Parameter Analysis.....	11
Data Analysis.....	12
DESIGN CONSIDERATIONS.....	20
Use of Design Curves.....	20
Sample Problem.....	22
DATA PRESENTATION.....	24
CONCLUSIONS.....	42
ACKNOWLEDGMENT.....	44

TABLE OF CONTENTS (concl)

REFERENCES.....	45
APPENDICES.....	46
APPENDIX A: Description and Explanation of the IBM 650 Computer Program Used to Calculate the Centerline Uncollided Flux from the End of a Finite Right-circular Cylinder.....	47
APPENDIX B: Description of IBM 650 Computer Program Used to Calculate the Error in Centerline Uncollided Flux Determination from the End of a Finite Right-circular Cylinder by the Use of an Equivalent Circular Plane Source...	58

INTRODUCTION

The cylinder is a shape quite frequently encountered in engineering work, and the nuclear field is no exception. Many reactors, many fuel elements, and many other sources of radiation have shapes approximating cylinders.

It is not uncommon to need to know the flux from the end of such a cylinder, whether the flux is composed of neutrons or gamma rays or both. This information is required for such reasons as the design of adequate shielding and for calculation of dose rates. To the author's knowledge, there is no method of calculation available at this time which can be performed without a computer in reasonable time periods and give answers with predictable accuracy.

An approximate solution has been developed by Rockwell (6) for determining upper and lower limits on the flux from the end of a cylinder. This technique, while bracketing the flux, in many cases provides such a large bracket that the actual flux is still very much in doubt.

An IBM 704 Computer code has been developed by Gillis et al. (3), which calculates the uncollided flux at any point outside a cylinder.

It is the purpose of this paper to develop empirical techniques enabling one to determine the centerline uncollided flux from the end of a finite cylinder without the aid of a computer.

NOMENCLATURE

Φ	Scalar flux ($\text{cm}^{-2} \text{sec}^{-1}$)
S_A	Source strength of plane source ($\text{cm}^{-2} \text{sec}^{-1}$)
S_V	Source strength of volume source ($\text{cm}^{-3} \text{sec}^{-1}$)
μ_i	Macroscopic cross section of <i>i</i> th shield material (cm^{-1})
μ_s	Macroscopic cross section of source material (cm^{-1})
t_i	Thickness of <i>i</i> th shield material (cm)
t_0	Thickness of source disk (cm)
a	Distance from end of cylinder to observation point (cm)
$\bar{\mu}$	$\sum_i^n \mu_i t_i / a$ (cm^{-1})
b_1	$\sum_i^n \mu_i t_i$
z	Effective self-attenuation distance (cm)
b_2	$b_1 + \mu_s z$
h	Cylinder height (cm)
b_3	$b_1 + \mu_s h$
h'	Cone height having same volume as cylinder (cm)
b_3'	$b_1 + \mu_s h'$
R_0	Cylinder radius (cm)
θ_1	$\tan^{-1} R_0 / a$
θ_2	$\tan^{-1} R_0 / (a + h)$
$N_{\text{MAX}} + 1$	Number of disks in cylinder
δ	Depression of equivalent circular plane source (cm)
θ_N	$\tan^{-1} R_0 / (a + N t_0 + \delta)$
θ_z	$\tan^{-1} R_0 / (a + z)$
$E_n(b)$	$b^{n-1} \int_b^\infty \frac{e^{-t}}{t^n} dt$ $n > 0$, $E_0(b) = \frac{e^{-b}}{b}$

THEORETICAL DEVELOPMENT

Problem

The equations for calculation of uncollided flux from some geometrically simple sources are developed in Rockwell and those used in this work are listed here. From a circular plane source (Fig. 1) of radius R_0 emitting S_A particles per square centimeter-second,

$$\Phi(a) = \frac{S_A}{2} \left\{ E_1(b_1) - E_1(b_1 \sec \theta) \right\} \quad (1)$$

From a truncated cone (Fig. 2) of height h emitting S_V particles per cubic centimeter-second the flux at P , the imaginary apex of the cone is,

$$\Phi(a) = \frac{S_V}{2\mu_s} \left\{ E_2(b_1) - \frac{E_2(b_1 \sec \theta)}{\sec \theta} - E_2(b_3) + \frac{E_2(b_3 \sec \theta)}{\sec \theta} \right\} \quad (2)$$

The flux from the end of a cylinder (Fig. 3) is not so easily obtained and must be calculated by approximation techniques. There are several approximate solutions available and these are listed and discussed. In all following discussion the orientation of the cylinder will be assumed to be such that the centerline is vertical and the detection point P is above the cylinder. All the solutions require that the point P be on the centerline of the cylinder. All solutions also require that the source S_V be of constant strength throughout the cylinder.

There are six parameters which must be considered in this problem area. Those associated with the cylinder are μ_s , R_0 , and h . The parameters associated with the shield are b_1 , a , and $\bar{\mu}$. The shield is assumed to be composed of slabs perpendicular to the cylinder centerline.

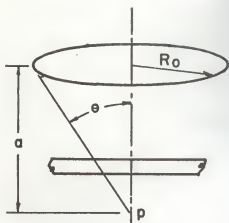


Fig.1. Circular plane source.

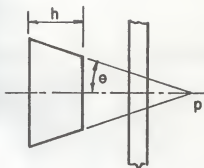


Fig. 2. Truncated right-circular cone source.

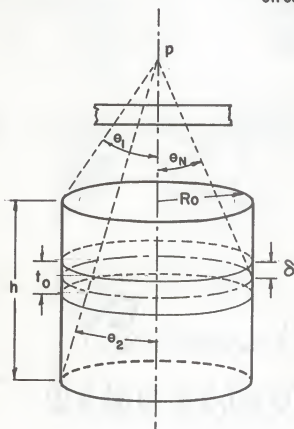


Fig.3. Right-circular cylindrical source viewed endwise

Solutions

Stacked Disk Solution. In order to determine empirical relationships for the flux, it was necessary to determine the flux accurately and this solution served that purpose. A cylinder is assumed to be made up of a series of thin stacked disks. The flux at P from each disk will be calculated by assuming each disk to be an equivalent circular plane source with $S_A = S_V t_o$. The shielding of all disks above the one under consideration must be considered so each disk will "see" a different amount of shielding.

The self-shielding of each disk is considered by locating the plane source some distance δ beneath the upper surface of the disk as shown in Fig. 3. Since the location of the plane source within the disk is actually a weighting function applied to the source distributed within the disk, δ is expected to be less than $t_o/2$ because the upper portion of the disk is more important due to the fact that it "sees" less shielding.

A second reason exists for choosing $\delta < t_o/2$; that being the desire to always make conservative calculations where possible exposure to nuclear radiation may be involved. As the plane source is moved closer to the upper surface of the disk, it "sees" less of the shielding in the disk than is actually the case so the resultant flux calculation will be too high. As the disks are made thinner, the neglected shielding in the source will decrease and the solution becomes more accurate.

The mathematical expression for the flux is

$$\Phi(a) = \frac{S_V t_o}{2} \sum_{N=0}^{NMAX} \left\{ E_1(b_1 + N\mu_s t_o + \mu_s \delta) - E_1[(b_1 + N\mu_s t_o + \delta\mu_s) \sec \theta_N] \right\}, \quad (3)$$

where \underline{NMAX} , $\underline{t_0}$, and $\underline{\delta}$ will be chosen to assure the calculated flux is within 1% higher than the true flux. Equation 3 is identical to Eq. A-1 in Appendix A which explains the computer code used to solve the equation.

Large Cone Approximation. This solution assumes the cylinder to be a truncated cone the same height as the cylinder with \underline{P} at the apex. The angle subtended by the cone is $\underline{\theta_1}$ on Fig. 3, and the cone is obviously larger than the cylinder it represents. The flux from this approximation is calculated by

$$\Phi(a) = \frac{S_V}{2\mu_s} \left\{ E_2(b_1) - \frac{E_2(b_1 \sec \theta_1)}{\sec \theta_1} - E_2(b_3) + \frac{E_2(b_3 \sec \theta_1)}{\sec \theta_1} \right\} \quad (4)$$

This solution provides an upper limit on the flux from the cylinder. Equation 4 is identical to Eq. A-3 in Appendix A which explains the computer code used to solve the equation.

Small Cone Approximation. This solution also assumes the cylinder to be a truncated cone which is the same height as the cylinder with \underline{P} at the apex. The angle subtended by the cone is $\underline{\theta_2}$ on Fig. 3, and the cone is obviously smaller than the cylinder it represents. The flux from this approximation is calculated by

$$\Phi(a) = \frac{S_V}{2\mu_s} \left\{ E_2(b_1) - \frac{E_2(b_1 \sec \theta_2)}{\sec \theta_2} - E_2(b_3) + \frac{E_2(b_3 \sec \theta_2)}{\sec \theta_2} \right\} \quad (5)$$

This solution provides a lower limit on the flux from the cylinder and when coupled with the large cone approximation provides a bracket on the expected flux. Equation 5 is identical to Eq. A-5 in Appendix A which explains the computer code used to solve the equation.

Equivalent Volume Cone Approximation. This solution also assumes the cylinder to be a truncated cone with \underline{P} at the apex. The angle subtended

by the cone is θ_1 on Fig. 3, and the height of the truncated cone is such that the volume is equal to that of the cylinder it represents. The flux from this approximation is calculated by

$$\Phi(a) = \frac{S_V}{2\mu_s} \left\{ E_2(b_1) - \frac{E_2(b_1 \sec \theta_1)}{\sec \theta_1} - E_2(b_3) + \frac{E_2(b_3 \sec \theta_1)}{\sec \theta_1} \right\} \quad (6)$$

Equation 6 is identical to Eq. A-4 in Appendix A which explains the computer code used to solve the equation.

Equivalent Circular Plane Source Approximation. This solution assumes that the cylinder can be represented by a single circular plane source the same radius as the cylinder. The equivalent source is assumed to be located somewhere within the space occupied by the cylinder it represents so that the shielding it "sees" is that of the cylinder within the confines of the cylinder. To allow for self-shielding within the source, the strength of the equivalent source must be considered in two parts. For cylinders with small mean free path height ($\mu_s h$) the equivalent source strength will be assumed to be $S_A = S_V h$. For cylinders with a mean free path height greater than some value K_1 which is chosen empirically, the source strength will be assumed to be $S_A = \frac{KS_V}{\mu_s}$. The flux from this approximation is calculated by

$$\Phi(a) = \frac{S_V h}{2} \left\{ E_1(b_2) - E_1(b_2 \sec \theta_2) \right\}, \text{ if } \mu_s h \leq K. \quad (7)$$

or

$$\Phi(a) = \frac{KS_V}{2\mu_s} \left\{ E_1(b_2) - E_1(b_2 \sec \theta_2) \right\}, \text{ if } \mu_s h > K. \quad (8)$$

Equations 7 and 8 are identical to Eqs. A-6 and A-7 respectively in Appendix A which explains the computer code used to solve the equations.

NUMERICAL ANALYSIS

Method of Solution

This problem has six parameters which may vary; R_0 , μ_g , h , \bar{h} , b_1 , and g . In order to consider all possible combinations of parameters adequately, a large number of problems had to be solved. To do this an IBM 650 Computer code was written which solved the problems by each of the five previously listed solutions. This code is described in Appendix A.

By proper choice of disk thickness the stacked disk solution could be used to solve the problem with any desired degree of accuracy. This solution was used to provide an answer accurate to within 1%. The choice of disk thickness to assure this accuracy will be discussed later.

The three conical approximate solutions were compared with the stacked disk solutions and the relative error of each solution was calculated. The results were examined in an effort to determine some simple method of empirically presenting the data to enable one to calculate the correct flux within some set limits of accuracy without the use of a computer.

The plane source approximation was used as a trial and error calculation to determine the self-absorption distance which forced the solution to approximate the stacked disk solution within specified limits. The results were examined in an effort to determine a simple empirical relationship between the self-absorption distance and the flux.

Preliminary Investigations

Accuracy Analysis of Stacked Disk Solution. Using the computer code, it was first necessary to determine the disk thickness which gave sufficient

accuracy. As the disks became thinner the solution became more accurate, so very thin disks were preferred. On the other hand, computer running time increased as disk thickness decreased since more disks were then required for any given problem. A compromise was made such that the flux was always calculated to within 1% of the asymptotic value, the result being always higher than the true value. The required disk thickness could then be determined for different combinations of parameters.

In order to better understand the problems associated with the work undertaken, it was necessary to approach the problems of disk thickness and location of the equivalent plane source within each disk in an oblique fashion. It was first assumed that the plane source was on the upper surface of each disk, i.e. $\delta = 0$, and disk thicknesses were determined. Problems solved with this choice of δ were quite lengthy, due to the necessity of using extremely thin disks since no self-absorption in each disk was considered. This extreme location of δ was used initially since the results would satisfy the original requirement that the flux always approach the correct flux from some higher value.

With the information provided from the initial set of problems, it was possible to compare the results with those obtained when δ was varied. Three facts were immediately apparent when these comparisons were made. First, the optimum location for δ was quite near $t_0/2$. Second, the optimum location for δ varied as the parameters of the cylinder and shield varied. Third, the major portion of the advantage of the depression of the plane source was observed as δ varied from 0 to $0.4t_0$. The choice was made for $\delta = 0.45t_0$ and proved to be satisfactory. The advantage of this depression of the plane source was a decrease in the number of disks

required for any given cylinder, the decrease being at least a factor of ten which saved considerable computer time.

In the search to determine the proper disk thickness for each problem, three parameters were shown to have an appreciable effect on the thickness necessary to provide the 1% accuracy required. The results of this search are shown in Table 1 with the variation of a single parameter from some intermediate value shown as the cause with the change of disk thickness while still maintaining 1% accuracy of the calculated flux shown as the effect.

Table 1. Effect on disk thickness required to determine flux within 1% of the asymptotic value as parameters are varied from intermediate values.

Cause	:	Effect
	:	
Increase b_1		Thicker
Increase R_0		Thicker
Increase μ_s		Thicker

The disk thickness was determined in terms of mean free paths, $\mu_s t_0$. Use of mean free paths makes it easier to explain the dependence on μ_s while not affecting the other results.

By the choice of δ , the location of the circular plane source within each disk representing the disk, some small amount of the shielding within each disk has not been considered. This was done, as previously explained, to force the flux calculation to always approach the asymptotic value from some higher value. Certainly one expects this neglected shielding to become less important as the total amount of shielding is increased. This expectation is borne out by the observed effect that increasing b_1 has on disk thickness.

In considering the dependence on R_0 , it is only logical to assume that to represent a disk by a plane the disk must "look like" a plane, that is, $R_0 \gg t_0$. This being the case, one expects that disks with larger radii could be thicker and still "look like" a plane. This expectation is borne out by the observed effect that increasing R_0 has on disk thickness.

The effect of μ_s on disk thickness is again one of geometry. As μ_s increases, the disk thickness in terms of mean free paths is expected to increase because this tends to hold the shape of the disk constant. If the thickness did not increase, the disk would approximate a plane even more closely than necessary. The expected results were observed and disk thickness did increase as μ_s increased.

Parameter Analysis. Having chosen δ it was possible to calculate the flux from cylinders whose parameters were chosen at random, as were the parameters of the shields. These problems were solved in an effort to determine which approximate method of solution or combination of methods showed the greatest promise as a tool to be eventually used in the simple empirical presentation of data which was desired.

The three conical solutions were shown to have little promise. As $\mu_s R_0$ decreased no single solution or average combination of the approximate conical solutions could provide accurate results. Errors were greater than a factor of 10 in some cases. The errors varied in such inconsistent fashion that no pattern which might make the application of correction factors to the approximate solution(s) feasible could be observed. In most cases the large cone approximation and the equivalent volume cone approximation were more nearly correct and the large cone approximation was the more reliable of these two because it always gave a conservative result.

The equivalent plane source approximation was chosen as the only approach which showed some promise of lending itself to the empirical fit of large amounts of data. It was observed that for large $\mu_s R_0$, the self-absorption distance in terms of mean free paths, $\mu_s z$, depended only on b_1 for a given cylinder height and it was decided to present the results as a family of curves for different $\mu_s h$ with $\mu_s z$ plotted versus b_1 .

It was possible at this point to choose a value for K , the mean free path cylinder height that fixed the constant source strength, for cylinders whose height exceeded K mean free paths. The artificial circular plane source having $S_A = S_V h$ kept increasing as h increased, although the flux from the cylinder did not. The self-absorption distance z necessarily increased as the plane source increased and these compensating effects were undesirable since the flux did not continue to increase. The value of K was fixed at 1.5 so that all cylinders more than 1.5 mean free paths tall were assumed to have an equivalent circular plane source strength such that $S_A = 1.5 S_V / \mu_s$. The plane source strength then fell into one of two categories: if $\mu_s h \leq 1.5$, $S_A = S_V h$; if $\mu_s h > 1.5$, $S_A = 1.5 S_V / \mu_s$. The figure of $\mu_s h = 1.5$ was chosen as the minimum value which could be used to fix a constant source strength without a risk of developing a negative z , which is not anticipated in the computer program. The minimum value was desired since the accuracy of the empirical relationships improved as the cylinder height used to fix a constant source strength decreased.

Data Analysis

Typical values for R_0 and μ_s were chosen and problems with varying \bar{H} , a , b_1 , and h were solved and the resultant curves in Figs. 4a and 4b were

determined. The self-absorption distance $\mu_s z$, expressed in terms of mean free paths, refers to the equivalent circular plane source which is assumed to replace the cylinder. Presentation of the data in this manner requires that $\mu_s z$ be dependent only on the shield mean free paths, b_1 , for a given cylinder height. This requirement is satisfied for large $\mu_s R_0$.

For the cases of small $\mu_s R_0$, marked deviation of $\mu_s z$ from that suggested by Figs. 4a and 4b was observed. In general, $\mu_s z$ increased as $\mu_s R_0$ first dropped below some critical value dependent on b_1 , and eventually decreased rapidly as $\mu_s R_0$ continued to decrease. Figure 5 indicates the area where fluxes may be calculated to within 10% of the actual value without the use of correction factors. As $\mu_s R_0$ exceeds the critical value shown for any b_1 , correction factors are not required.

The maximum deviation of $\mu_s z$ from the values predicted by Figs. 4a and 4b is observed for large $\bar{\mu}$. For a given value of $\mu_s R_0$ the deviation was greater for smaller μ_s as $\bar{\mu}$ was held constant. The relative deviation was slightly dependent on $\mu_s h$ and quite dependent on b_1 . It was necessary to develop correction factors for $\mu_s z$ which depend on b_1 , $\bar{\mu}$, and μ_s . This has been done in Figs. 6 through 12. These correction factors were determined by assuming cylinders having $\mu_s h = 2$. and the results are most accurate for this case. For values of $\mu_s h$ not equal to two the error in the calculated flux for small $\mu_s R_0$ increases. Largest errors are noted when μ_s is small, R_0 is small, and $\bar{\mu}$ is large. Errors are greatest for the smallest $\mu_s h$. Errors are positive, i.e. the empirically determined flux is greater than the flux determined by the stacked disk solution, for most cases, and the estimated maximum negative error is <25%. The estimated maximum

positive error is $< 175\%$ and these extreme errors apply only in isolated cases. Table 2 lists the estimated maximum errors anticipated for varying $\underline{\mu}_s$ and varying $\underline{\mu}_{sh}$ at values of $\underline{\mu}_{sh}$ other than 2. The comparable errors resulting from the use of the large cone approximation are included in Table 2. Appendix B explains the computer program used to calculate the error in flux determination by the empirical method.

Table 2. Study of maximum percentage errors in flux determination compared to stacked disk flux determination, by the curves in this paper and by the large cone approximation for varying source and shield parameters.

		Percentage errors in flux determination																																				
		$\bar{\mu} = 0.02$				$\bar{\mu} = 0.1$				$\bar{\mu} = 1.0$				$\bar{\mu} = 4.0$																								
μ_s	μ_{sh}	b_1	Curves : Large : cone : paper * : approx.	Curves : in this : paper * : approx.	Large : cone : approx.	Curves : in this : paper * : approx.	Large : cone : approx.	Curves : in this : paper * : approx.	Large : cone : approx.	Curves : in this : paper * : approx.	Large : cone : approx.	Curves : in this : paper * : approx.	Large : cone : approx.	Curves : in this : paper * : approx.																								
0.02	0.25	0.1	36.7	228.9	90.5	854.5	145.7	1312.5	155.8	1213.1	1.0	1.5	23.6	20.0	3.2	8.9	4.0	0	3.2	29.6	756.3	139.9	97.1	531.1	779.8													
		10	1.1	-3.9	0.1	10.6	19.4	114.1	57.3	330.8	30	0.7	-5.0**	4.5	39.0	25.0	138.9																					
0.02	1.00	0.1	10.3	690.7	10.9	2370.8	9.8	2756.6	10.2	2498.1	1.0	0.4	79.1	1.3	362.5	7.0	2118.8	3.2	2021.1	3.2	1539.2	1.0	-2.1	4.0	21.1	-4.5	97.8	4.0	8.2	10	2.6	8.2	356.1	995.7	432.8			
		10	2.6	8.2	-4.7	40.0	-6.8	356.1	-5.8	995.7	30	-2.0	9.3	-7.3	127.8	-6.5	432.8																					
0.02	1.25	0.1	10.7	785.5	8.5	2645.7	5.0	2943.8	5.1	2664.4	1.0	0.4	92.1	1.2	414.8	2.9	2367.6	-2.6	2217.9	2.8	1727.6	1.0	4.3	2.5	24.1	4.0	8.2	10	0.3	8.2	407.6	1128.5	494.5					
		10	0.3	8.2	-2.7	47.0	-8.3	407.6	-10.4	1128.5	30	0.6	14.0	-7.1	148.2	-9.1	494.5																					
0.02	1.50	0.1	2.9	859.9	-1.8	2851.0	-6.5	3071.6	-6.3	2777.8	1.0	-1.8	103.0	-5.0	456.2	-7.6	2554.1	-13.8	2358.6	2.8	1727.6	1.0	0.6	26.9	4.0	10.6	10	1.4	10.6	448.5	1231.7	543.3						
		10	1.4	10.6	-4.5	53.0	-15.7	448.5	-20.2	1231.7	30	0.6	16.1	-12.1	164.7	-17.2	543.3																					
0.02	1.75	0.1	4.3	918.0	-0.4	3004.5	-4.8	3160.2	-4.6	2856.5	1.0	0.4	111.9	-1.4	488.9	-2.6	2693.9	-13.8	2459.9	2.8	1727.6	1.0	1.4	29.8	4.0	11.4	10	0.2	11.4	480.7	1311.7	581.7						
		10	1.4	29.8	-1.7	137.5	-6.1	1070.7	-8.0	1977.9	30	0.2	58.1	-6.6	178.1	-6.7	581.7																					

Table 2. (cont).

Percentage errors in flux determination											
$\bar{\mu} = 4.0$											
$\bar{\mu} = 1.0$											
$\bar{\mu} = 0.1$											
$\bar{\mu} = 0.02$											
μ_s	μ_{sh}	b_1	Curves in this paper *	Large cone approx.	Curves in this paper *	Large cone approx.	Curves in this paper *	Large cone approx.	Curves in this paper *	Large cone approx.	Curves in this paper *
0.02	3.00	0.1	8.1	1064.9	4.2	3353.1	-0.6	3338.0	-0.6	3014.3	3014.3
		1.0	4.8	136.4	9.6	572.7	11.2	3013.9	4.8	2675.6	2675.6
		4.0	4.2	38.1	13.1	166.3	18.8	1239.0	19.5	2230.0	2230.0
		10	0.3	15.4	11.1	72.6	23.2	563.3	24.6	1510.0	1510.0
		30			6.6	24.7	22.0	213.7	29.6	679.5	679.5
0.05	0.25	0.1	13.1	92.4	57.5	341.5	107.4	509.3	113.3	463.9	463.9
		1.0	-0.1	9.3	7.8	46.9	58.9	299.8	96.0	292.3	292.3
		4.0	0.02	5.2	0.4	11.9	20.5	108.1	63.9	203.6	203.6
		10	0.3	-4.7	0.2	3.5	6.1	45.9	26.9	130.0	130.0
		30			0.3	-7.0	0.3	15.6	9.9	55.4	55.4
0.05	1.00	0.1	3.3	289.9	14.4	973.9	18.4	1099.1	17.3	988.6	988.6
		1.0	-1.1	32.4	3.2	152.1	7.2	869.1	9.1	806.2	806.2
		4.0	0.3	8.7	-2.4	40.2	-1.5	337.9	14.2	625.1	625.1
		10	2.7	3.4	-1.1	16.1	-6.2	149.2	-5.4	411.1	411.1
		30			-0.2	1.4	-6.8	52.8	-3.2	180.4	180.4
0.05	1.25	0.1	5.4	332.2	13.1	1090.4	14.1	1176.5	13.0	1057.2	1057.2
		1.0	2.5	38.2	5.9	175.9	4.9	975.0	3.9	888.8	888.8
		4.0	2.9	9.7	0.5	47.4	-2.3	387.5	10.3	708.4	708.4
		10	0.8	2.6	1.6	19.0	-6.1	172.9	-8.0	470.6	470.6
		30			1.8	4.6	-5.4	62.0	-3.5	208.8	208.8
0.05	1.50	0.1	0.3	365.9	4.3	1177.8	2.2	1229.4	0.7	1104.2	1104.2
		1.0	2.4	43.1	2.6	195.1	-4.5	1054.6	-7.6	948.0	948.0
		4.0	3.3	10.7	-1.1	53.3	-9.6	425.2	-1.0	767.3	767.3
		10	0.4	4.2	1.3	21.7	-11.6	191.5	-16.9	515.1	515.1
		30			0.9	5.3	-8.4	69.6	-9.3	230.9	230.9

Table 2. (cont).

μ_s	μ_{sh}	b_l	Percentage errors in flux determination																																						
			$\bar{\mu}$	0.02	Curves in this paper *	Large cone approx.	Curves in this paper *	Large cone approx.	$\bar{\mu}$	0.1	Curves in this paper *	Large cone approx.	$\bar{\mu}$	1.0	Curves in this paper *	Large cone approx.																									
0.05	1.75	0.1	0.8	392.5	5.5	1243.2	3.7	1266.2	2.0	1136.8	1.5	210.5	-0.1	1114.5	-2.2	990.7	4.0	2.6	47.2	1.0	58.3	-2.4	455.9	8.9	814.8	10	-1.5	4.1	2.3	24.0	-3.7	206.8	-7.1	551.3	30	3	7.0	1.9	76.0	-3.1	248.9
0.05	3.00	0.1	3.7	460.7	10.2	1392.5	5.5	1340.1	0.4	1202.4	1.8	59.4	13.7	251.2	11.5	1081.8	4.0	1.4	15.7	9.4	532.8	20.5	72.7	28.1	923.4	10	-3.2	6.2	6.5	30.9	19.2	246.8	18.0	640.2	30	3	9.5	0.8	93.8	14.3	295.7
0.1	0.25	0.1	5.5	46.3	28.7	169.3	60.9	241.7	69.2	214.6	1.0	-0.3	2.1	23.5	36.5	131.1	4.0	0.5	4.0	4.0	5.9	9.1	54.1	31.0	95.1	10	0.1	-4.9	0.2	1.0	1.5	22.7	11.0	62.7	30	3	-7.9	-0.02	7.6	1.8	27.3
0.1	1.00	0.1	3.8	150.0	4.7	498.1	3.4	541.2	14.8	481.1	0.7	16.4	-0.6	78.4	11.7	443.7	12.2	0.8	4.6	4.6	20.4	-0.9	174.9	4.9	314.4	10	0.5	1.2	0.02	7.8	-6.0	76.6	-7.5	209.4	30	3	-1.4	-3.3	26.7	-8.5	92.3
0.1	1.25	0.1	7.4	173.4	4.8	560.3	5.9	581.4	11.5	516.8	1.1	19.4	2.7	91.4	12.8	500.4	6.6	4.0	4.9	4.9	24.1	-1.6	202.2	2.7	359.0	10	3.2	0.5	3.0	9.3	-4.8	89.4	-9.2	241.3	30	3	11.8	-1.0	31.5	-8.2	107.7

Table 2. (cont).

		Percentage errors in flux determination													
		$\mu=0.02$				$\mu=0.1$				$\mu=1.0$				$\mu=4.0$	
μ_s	μ_h	b_l	Curves : in this : paper * :	Large : cone : approx. :	Curves : in this : paper * :	Large : cone : approx. :	Curves : in this : paper * :	Large : cone : approx. :	Curves : in this : paper * :	Large : cone : approx. :	Curves : in this : paper * :	Large : cone : approx. :	Curves : in this : paper * :	Large : cone : approx. :	
0.1	1.50	0.1	4.5	192.2	-2.2	607.1	-4.2	609.1	0.6	541.3	-4.7	469.3	0.6	541.3	
		1.0	5.4	21.9	0.6	102.0	2.9	541.9	-4.7	469.3	-6.3	391.4	0.1	492.7	
		4.0	4.5	5.2	27.3	2.6	-7.2	223.3	-7.2	391.4	-16.1	267.0	1.8	417.3	
		10	3.2	1.8	3.1	10.8	-8.2	100.1	-8.2	267.0	-12.5	120.4	1.8	286.6	
		30			3.0	1.7	-2.1	35.8	-2.1	120.4			1.8	130.5	
0.1	1.75	0.1	4.5	207.3	-1.6	642.4	-3.0	628.3	1.5	558.4	7.3	492.7	1.5	558.4	
		1.0	3.0	24.2	2.1	110.9	7.3	574.7	0.1	492.7	-0.7	417.3	0.1	492.7	
		4.0	1.9	5.9	2.8	30.1	-0.7	240.7	1.8	417.3	-2.4	286.6	1.8	417.3	
		10	0.9	1.7	2.6	11.9	-2.4	108.7	-7.4	286.6	0.7	130.5	-7.4	286.6	
		30			1.7	2.8	0.7	39.2	-5.3	130.5			-5.3	130.5	
0.1	3.00	0.1	5.9	247.0	2.4	723.4	1.2	667.2	6.2	592.9	20.9	542.9	6.2	592.9	
		1.0	-0.3	31.1	7.5	135.2	18.6	650.8	17.1	542.9	15.4	477.5	17.1	542.9	
		4.0	2.0	7.9	5.6	38.4	15.4	285.2	28.4	477.5	12.2	337.5	28.4	477.5	
		10	-1.3	2.8	3.0	15.7	12.2	132.5	20.4	337.5	1.0	158.2	20.4	337.5	
		30			0.2	4.1	1.0	49.7	18.1	158.2			18.1	158.2	
1.0	0.25	0.1	0.1	4.3	-0.6	15.8	1.0	14.9	1.1	7.0	0.3	4.3	1.1	7.0	
		1.0	-0.1	0.07	-0.06	2.1	0.3	13.0	-0.8	4.3	0	6.5	-0.8	4.3	
		4.0	0.1	2.8	0	0.4	-0.2	5.1	6.5	6.5	2.0	5.6	6.5	6.5	
		10	-0.3	-5.3	-0.2	-1.2	-0.2	2.0	-0.4	5.6	0.5	2.5	-0.4	5.6	
		30			-0.1	-9.0	-0.4	0.5	-0.5	2.5			-0.5	2.5	
1.0	1.00	0.1	5.6	15.7	-0.6	50.9	-0.6	34.1	-0.8	23.1	7.9	21.4	-0.8	23.1	
		1.0	1.9	1.4	1.9	7.9	-2.1	43.4	-3.3	21.4	1.8	25.2	-3.3	21.4	
		4.0	1.0	0.8	1.0	1.8	-0.5	18.3	-3.9	25.2	0.3	20.3	-3.9	25.2	
		10	0.3	0.9	-0.2	0.3	-1.2	7.7	-3.4	20.3	0.3	9.3	-3.4	20.3	
		30			-0.9	-4.2	-1.6	2.5	-2.7	9.3			-2.7	9.3	

Table 2. (concl)

		Percentage errors in flux determination														
		$\bar{\mu} = 0.02$				$\bar{\mu} = 0.1$				$\bar{\mu} = 1.0$				$\bar{\mu} = 4.0$		
μ_s	μ_{gh}	b_1	Curves in this paper *	Large cone approx.	Curves in this paper *	Large cone approx.	Curves in this paper *	Large cone approx.	Curves in this paper *	Large cone approx.	Curves in this paper *	Large cone approx.	Curves in this paper *	Large cone approx.	Curves in this paper *	Large cone approx.
1.0	1.25	0.1	11.0	18.6	3.5	58.6	3.3	37.8	3.1	26.5						
		1.0	5.7	1.7	6.0	9.4	1.3	50.3	-0.5	25.7						
		4.0	4.1	0.3	4.3	2.2	2.7	21.6	-1.5	30.0						
		10	2.5	-0.2	2.4	0.4	1.5	9.2	-1.1	24.1						
		30			1.6	-2.0	0.9	3.0	-0.3	11.1						
1.0	1.50	0.1	13.4	21.1	3.0	64.8	1.6	40.7	1.2	29.1						
		1.0	7.4	2.0	7.4	10.8	-0.1	55.9	-2.9	29.2						
		4.0	4.4	0	5.3	2.6	2.7	24.5	-3.0	34.1						
		10	2.7	1.3	2.9	0.4	1.4	10.3	-2.4	27.0						
		30			2.1	-2.2	0.8	3.2	-0.9	12.3						
1.0	1.75	0.1	9.0	23.3	1.4	69.7	1.1	42.8	1.1	31.0						
		1.0	2.8	2.2	3.9	12.0	0.5	60.4	-1.6	31.9						
		4.0	2.1	0.2	2.4	2.9	2.8	27.0	-0.7	37.5						
		10	-0.4	0.4	0.9	0.8	1.2	11.7	-0.1	30.1						
		30			0	-1.1	-0.2	3.9	-0.3	14.0						
1.0	3.00	0.1	1.7	29.9	0.3	82.1	2.3	47.8	2.1	35.6						
		1.0	-6.2	3.0	-2.2	15.7	4.2	71.9	3.7	38.8						
		4.0	-4.4	0.4	-3.1	3.7	4.9	34.1	7.2	46.3						
		10	-3.4	0.6	-3.0	1.2	1.7	15.3	7.1	38.4						
		30			-2.5	-1.2	-1.3	5.0	2.8	18.0						

* The interpolation required to determine the self-absorption distance may give rise to errors in the flux determination which exceed these estimated maximum errors. In no case is the error expected to increase by more than 5%.

** For large $\bar{\mu}$, i.e. large b_1 and small $\bar{\mu}$, the limitations of the computer were such that the large cone approximate calculation of flux was less than the stacked disk solution.

DESIGN CONSIDERATIONS

Use of Design Curves

The following curves are to be used to determine the location or self-absorption distance of a circular plane source assumed to represent a cylinder for purposes of calculating the centerline uncollided flux at some point \underline{P} , at distance \underline{a} beyond an end of the cylinder. The self-absorption distance is measured from the end of the cylinder closest to \underline{P} . Necessary input data are $\underline{\bar{\mu}}$, \underline{a} , $\underline{\mu}_s$, \underline{R}_0 , \underline{h} , and \underline{b}_1 . The following step-by-step procedure enables one to determine the self-absorption distance and the resultant flux. The following limits on the values of the parameters must be observed:

$$\begin{aligned} \underline{R}_0 &\geq 1 \text{ cm} \\ 0.1 &\leq \underline{b}_1 \leq 40 \\ 0.02 \text{ cm}^{-1} &\leq \underline{\mu}_s \\ 0.02 \text{ cm}^{-1} &\leq \underline{\bar{\mu}} \end{aligned} .$$

To determine the self-absorption distance proceed as follows:

Step 1. Calculate $\underline{\mu}_s h$.

Determine $\underline{\mu}_s z$ from Fig. 4a or 4b.

Step 2. Calculate $\underline{\mu}_s R_0$.

From Fig. 5 determine necessity of correction factor application. If correction factor is necessary go to step 3; if not, go to step 6.

Step 3. Using Figs. 6b, 7b, 8b, 9b, 10b, 11b, or 12b

select the Figures at the \underline{b}_1 values immediately larger and smaller than the given \underline{b}_1 . From these two Figures determine a relation to the appropriate \underline{F}_1 , \underline{G}_1 , \underline{H}_1 , \underline{J}_1 ,

\underline{K}_1 , \underline{L}_1 , or \underline{M}_1 curves. For example, at $\underline{b}_1 = 4$, on Fig. 8b at $\underline{\mu} = 0.3$ and $\underline{\mu}_s = 0.1$ a location between \underline{H}_2 and \underline{H}_3 is observed approximately one-third of the distance from \underline{H}_2 towards \underline{H}_3 .

- Step 4. With the relations determined in Step 3, use Figs 6a, 7a, 8a, 9a, 10a, 11a, or 12a as appropriate, and by interpolation determine correction factors at the two values for \underline{b}_1 used in Step 3.
- Step 5. Interpolating between \underline{b}_1 values, determine correction factor, \underline{CF} , to be used at the given \underline{b}_1 , and multiply \underline{CF} by $\underline{\mu}_s z$ which is then the $\underline{\mu}_s z$ to be used in succeeding steps.
- Step 6. Calculate $\sec \theta_z$ and \underline{z} from $\underline{\mu}_s z$,
 where $\sec \theta_z = \sqrt{1 + \frac{R_o^2}{(a+z)^2}}$.
- Step 7. Calculate $b_2 = b_1 + \underline{\mu}_s z$.
 Calculate $\{E_1(b_2) - E_1(b_2 \sec \theta_z)\}$,
 where $E_1(x) = -0.5772 - \ln x + x - \frac{x^2}{4} + \frac{x^3}{18} \dots$
 if $x < 1$, Refs. (1, 2, 6).
 $E_1(x) = \frac{e^{-x}}{x} \left\{ \frac{0.251 + 2.335x + x^2}{1.082 + 3.331x + x^2} \right\}$,
 if $x \geq 1$, Ref. (3).
- Step 8. If $\underline{\mu}_s h \leq 1.5$, $S_A = S_V h$
 If $\underline{\mu}_s h > 1.5$, $S_A = S_V \left(\frac{1.5}{\underline{\mu}_s} \right)$
- Step 9. $\Phi(a) = \frac{S_A}{2} \{E_1(b_2) - E_1(b_2 \sec \theta_z)\}$

If the flux is desired at some point \underline{P} not on the centerline of the cylinder a conservative estimate can be obtained by assuming the point \underline{P} is on the centerline of the cylinder at the same vertical distance above

the source, and solving the problem in the manner outlined above.

Sample Problem

The following problem will serve to illustrate the use of the design curves. The parameter values have been assumed to be as follows:

$$\mu_s = 0.07, \bar{\mu} = 0.3, b_1 = 6, R_0 = 10 \text{ cm}, h = 40 \text{ cm}, a = 20 \text{ cm}.$$

Step 1. $\mu_s h = 2.8$

From Fig. 4b, $\mu_z z = 0.497$

Step 2. $\mu_s R_0 = 0.7$ From Fig. 5, correction factor is necessary.

Step 3. From Fig. 8b, observe a location between

H_2 and H_3 close to H_3 .

From Fig 9b, observe a location between

J_1 and J_2 close to J_2 .

Step 4. From fig. 8a, by interpolation, the correction factor is estimated as 0.97. From Fig. 9a, by interpolation, the correction factor is estimated as 1.01.

Step 5. Correction factor is 0.983 for $b_1 = 6$.

Corrected $\mu_z z$ is 0.489.

Step 6. $z = 6.96 \text{ cm}$.

$\sec \theta_z = 1.0665$.

Step 7. $b_2 = 6.489$.

$b_2 \sec \theta_z = 6.920$.

$E_1(6.489) = 2.078 \times 10^{-4}$.

$E_1(6.921) = 1.273 \times 10^{-4}$.

Step 8. $S_A = 21.428 \text{ cm}^{-2} \text{ sec}^{-1}$

Step 9. $\Phi(a) = 8.625 \times 10^{-4} \text{ cm}^{-2} \text{ sec}^{-1}$

The stacked disk solution to this problem is $7.8 \times 10^{-4} \text{ cm}^{-2} \text{ sec}^{-1}$.
The error in the empirical solution is 10.6%. The error in the large
cone approximate solution is 64.7%.

DATA PRESENTATION

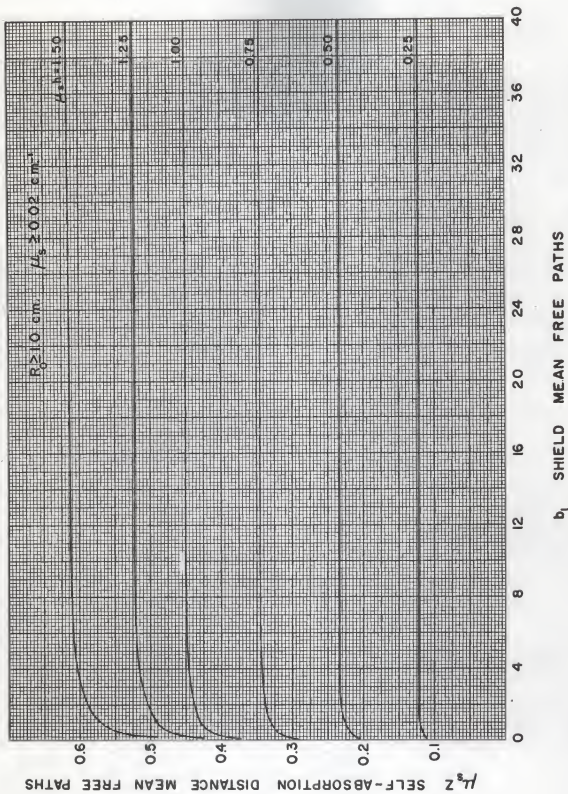


Fig. 4 a. Equivalent circular plane source self-absorption distance for $\mu_s h \leq 1.5$

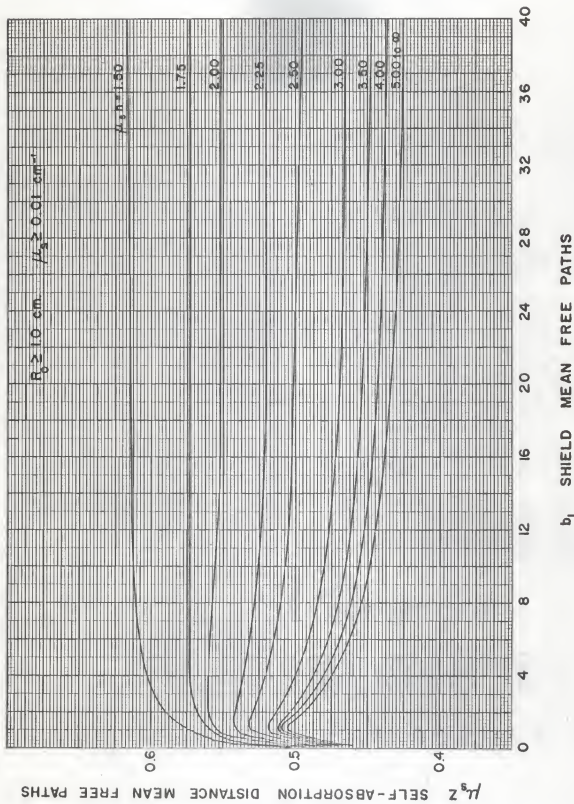


Fig. 4b. Equivalent circular plane source self-absorption distance for $\mu_s h > 1.5$

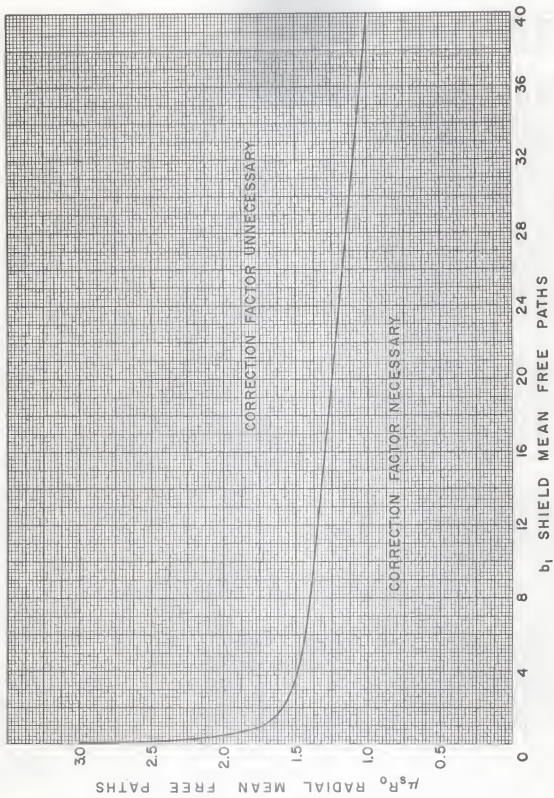


Fig. 5. Correction factor applicability.

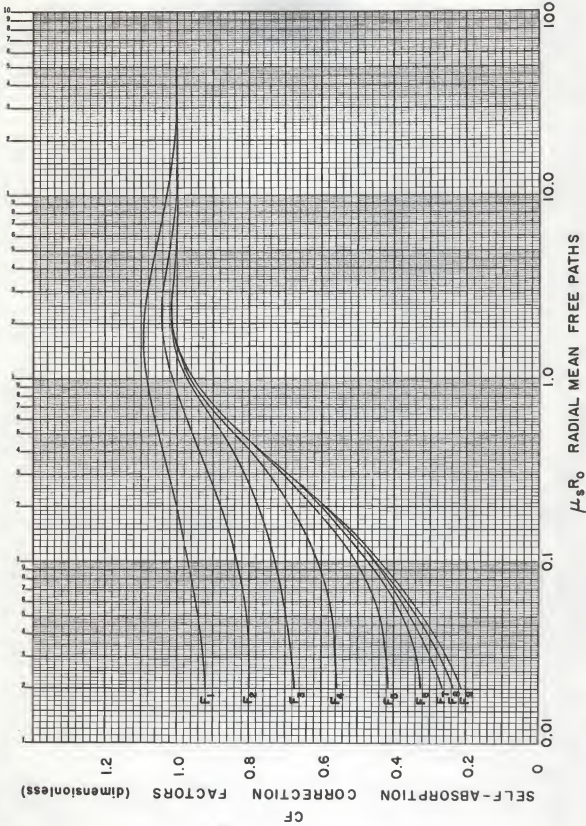


Fig. 6a. Correction factors for equivalent circular plane source self-absorption distance for $b_1=0.1$.

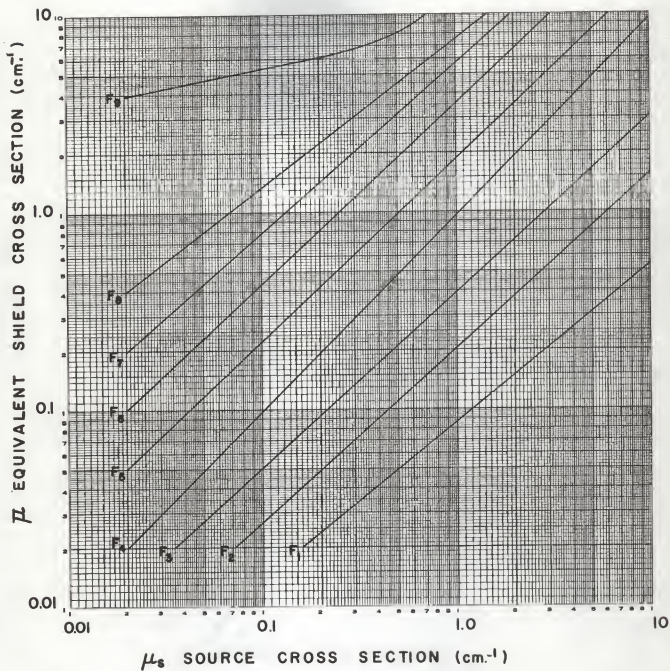


Fig. 6b. Source and shield cross sections correlation for $b_1 = 0.1$.

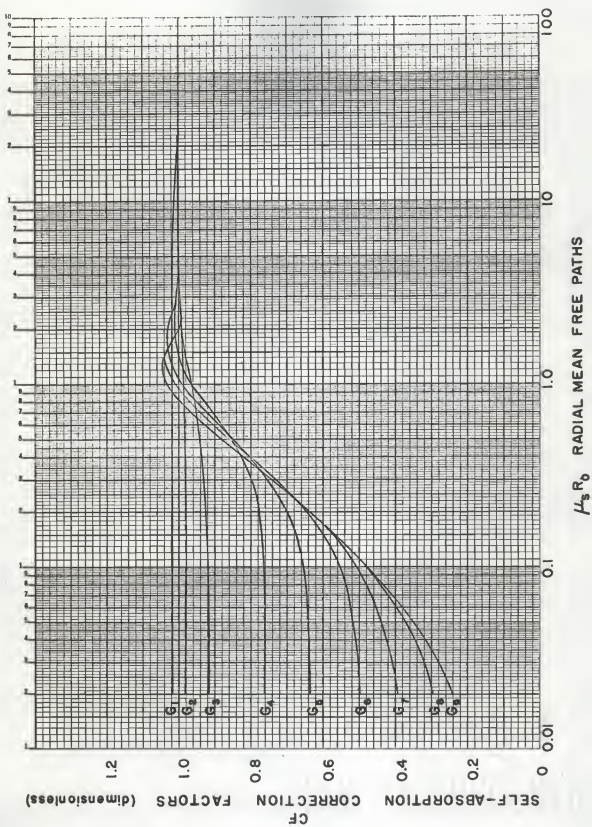


Fig. 7a. Correction factors for equivalent circular plane source self-absorption distance for $b_s = 1.0$.

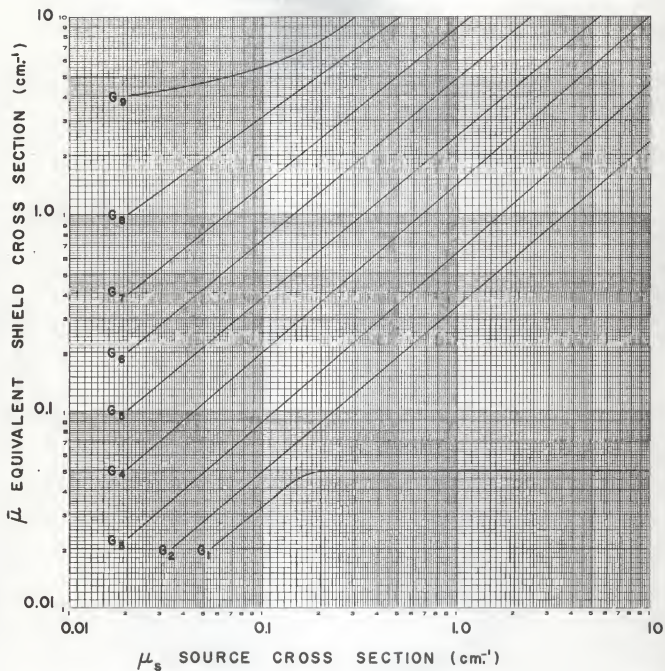


Fig. 7b. Source and shield cross sections correlation for $b_1 = 1.0$.

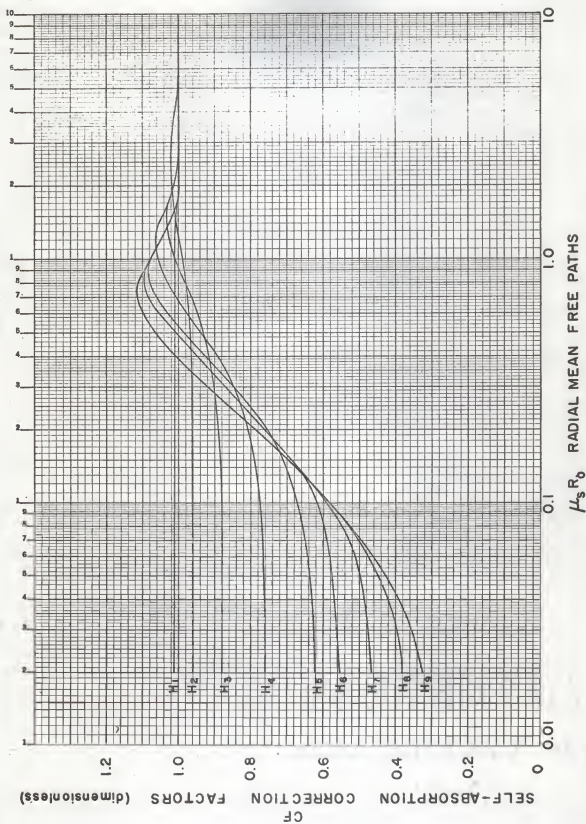


Fig. 8a. Correction factors for equivalent circular plane source self-absorption distance for $b=4.0$.

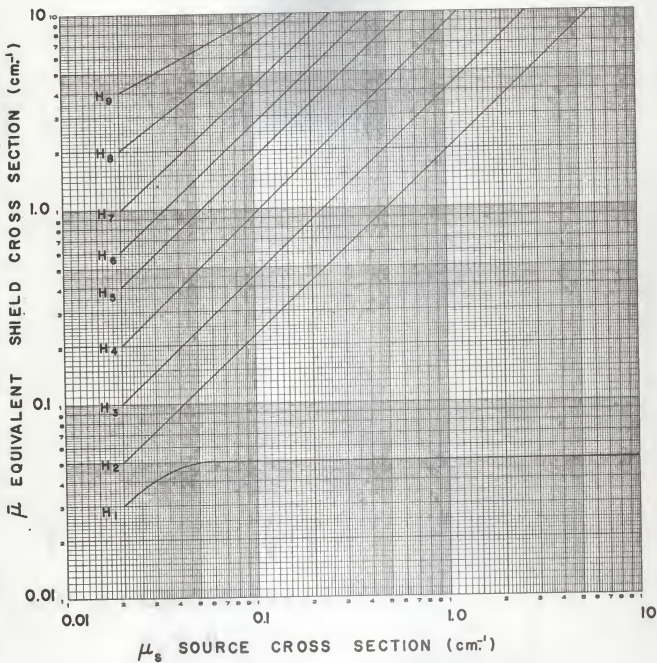


Fig. 8b. Source and shield cross sections correlation for $b_1 = 4.0$.

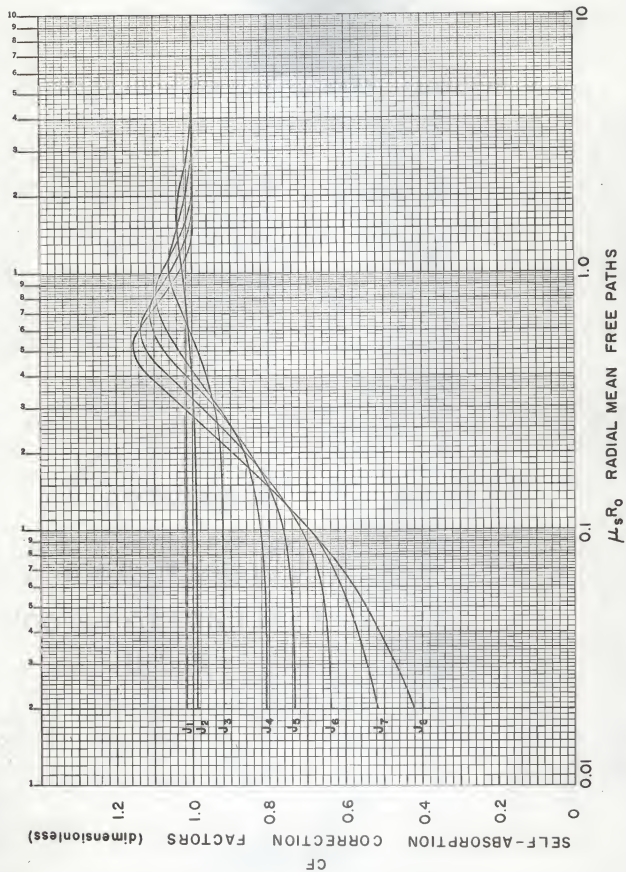


Fig. 9a. Correction factors for equivalent circular plane source self-absorption distance for $b_1 = 10$.

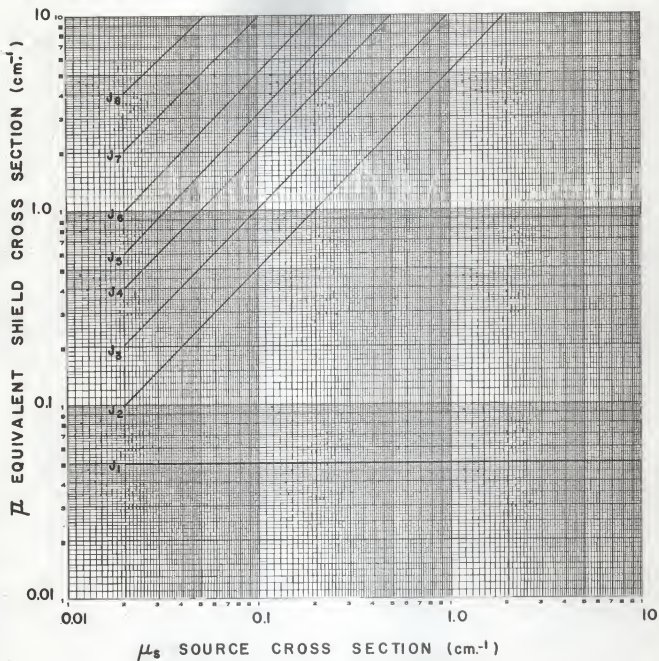


Fig. 9b. Source and shield cross sections correlation for $b_1 = 10$.

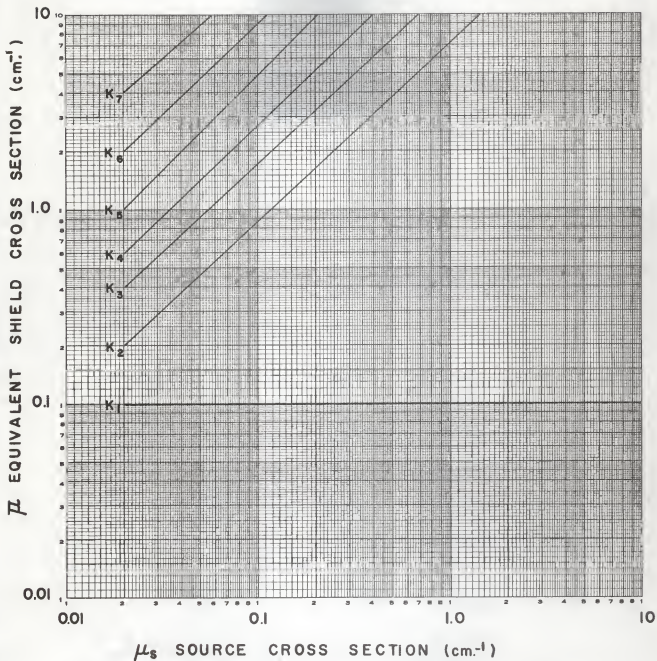


Fig. 10b. Source and shield cross sections correlation for $b=20$.

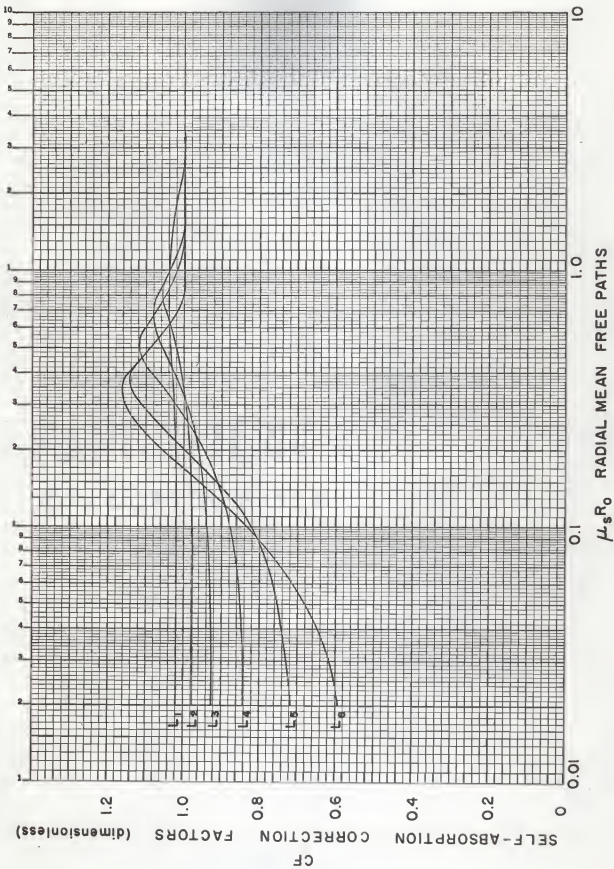


Fig. 11a. Correction factors for equivalent circular plane source self-absorption distance for $b_1 = 30$.

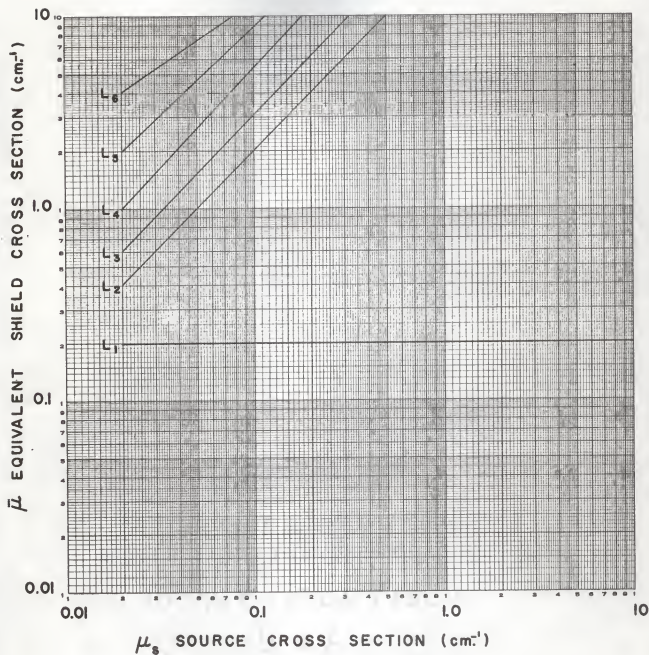


Fig. 11b. Source and shield cross sections correlation for $b_1 = 30$.

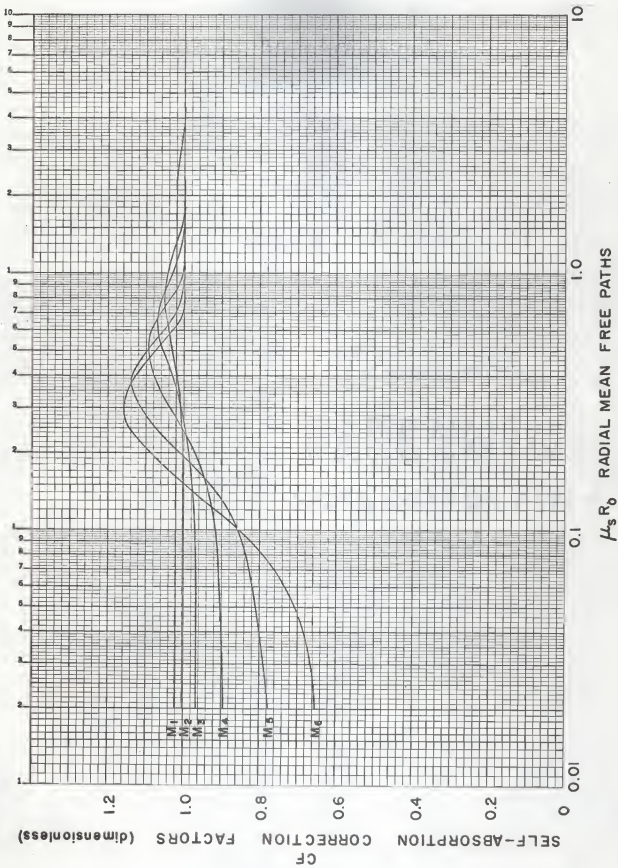


Fig. 12a. Correction factors for equivalent circular plane source self-absorption distance for $b_1=40$.

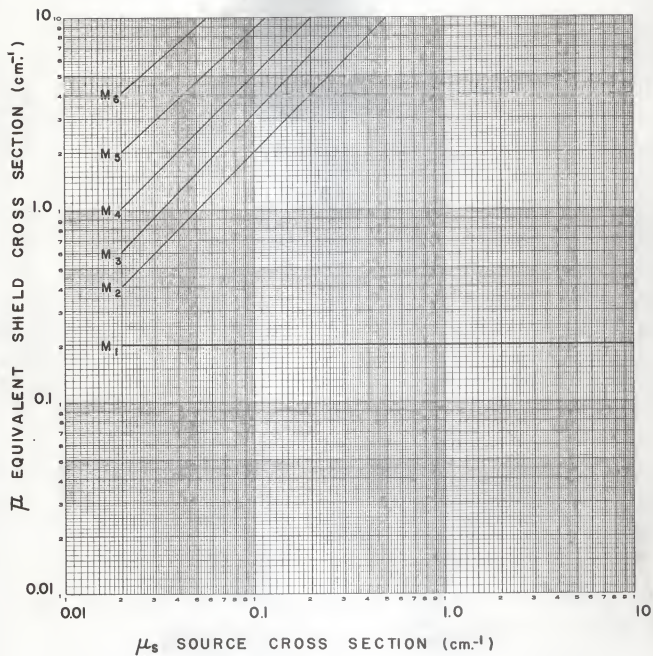


Fig. 12b. Source and shield cross sections correlation for $b_1=40$.

CONCLUSIONS

The largest errors in determination of fluxes by use of the curves presented in this paper will occur in the region where correction factors are necessary, due to the interpolation required to determine correction factors. Even so, this is the region where the greatest benefit is derived from this work, for it is here that currently used conical approximations are most in error.

For any given cylinder height, h , the cylinder ceases to look like a disk and becomes a slender rod as R_0 decreases. Similarly, for a fixed mean free path height, $\mu_g h$, as μ_g decreases the cylinder becomes longer and for a fixed radius the cylinder again appears rod-like. Certainly the artificial nature of the plane source approximation would be expected to have adverse effects in this region, if at all, and the correction factors necessary for small $\mu_g R_0$ were no surprise although their shape could not be anticipated.

An empirical solution similar to the one presented herein is presented in Rockwell (6) which enables one to determine the flux from the side of a cylinder by approximating the cylinder by a line source located within the cylinder. This empirical solution provides a method amenable to hand calculation to reproduce the results shown by Taylor and Obenshain (7). This original work is applicable only for cylinders having $h \gg R_0$ and $h > 1/\mu_g$. These limitations are not mentioned by Rockwell and therefore his empirical solution may be frequently applied in instances which exceed the restrictions placed on the original data.

It is recommended that work be done in the area of accurate flux solutions from the side of a cylinder for cases excluded by Taylor and Obenshain (7), and that an effort be made to combine the results. Further effort should be

made to present these results in some empirical form which lends itself to hand calculation. In particular, it is recommended that an effort be made to present the results in a manner analogous to that used in this paper.

ACKNOWLEDGMENT

The author wishes to express his gratitude to Dr. William R. Kimel, Head of the Department of Nuclear Engineering, for his encouragement and help throughout this course of study. Sincere thanks are extended to Mr. John R. Fagan of the Kansas State University Nuclear Engineering Staff for his guidance, to Professor R. C. Bailie and to fellow student R. E. Kaiser for their help in computer programming techniques.

REFERENCES

- (1) Goldstein, Herbert.
Fundamental Aspects of Reactor Shielding.
Reading: Addison-Wesley, 1959.
- (2) Grotenhuis, M.
Lecture Notes on Reactor Shielding.
ANL-6000 (TID - 4500, 14th Ed.), 1959.
- (3) Gillis, P.A., T.J. Lawton, and K.W. Brand.
Span -2 -- An IBM 704 Code to Calculate Uncollided
Flux Outside a Circular Cylinder.
WAPD-TM-176, 1959.
- (4) Gillis, P. A.
Spic -1 -- An IBM 704 Code to Calculate the Neutron Distribution
Outside a Right-Circular Cylindrical Source.
WAPD-TM-196, 1959.
- (5) Hastings, C.
Approximations for Digital Computers.
Princeton: Princeton University Press, 1955.
- (6) Rockwell, T., III.
Reactor Shielding Design Manual.
Princeton: Van Nostrand, 1956.
- (7) Taylor, J. J., and R. B. Obenshain.
Flux from Homogeneous Cylinders Containing Uniform
Source Distributions. WAPD-213, 1953.

APPENDICES

APPENDIX A

Description and Explanation of the IBM 650 Computer Program
Used to Calculate the Centerline Uncollided Flux
from the End of a Finite Right-circular Cylinder

This program was written to calculate the centerline uncollided flux from the end of a finite cylinder, both accurately and by existing approximation methods, and to calculate the self-absorption distance of an equivalent source. This program was written in Soap II computer language using floating point operations. The logic diagram and the object program are given in this appendix.

The accurate solution is designated FLUX and the solution programmed was

$$\Phi(a) = \frac{S_V t_0}{2} \sum_{N=0}^{NMAX} \left\{ E_1(b_1 + (N+0.45) \mu_s t_0) - E_1[(b_1 + (N+0.45) \mu_s t_0) \sec \theta_N] \right\} \quad (A-1)$$

$$\text{where } \sec \theta_N = \sqrt{1 + \frac{R_0^2}{(a + (N+0.45) t_0)^2}} \quad (A-2)$$

Equation A-1 is derived as Eq. 3, the stacked disk solution on page 5, with δ set at 0.45.

The solution to the large cone approximation was designated FLUXB and the solution programmed was

$$\Phi(a) = \frac{S_V}{2\mu_s} \left\{ E_2(b_1) - \frac{E_2(b_1 \sec \theta_1)}{\sec \theta_1} - E_2(b_3) + \frac{E_2(b_3 \sec \theta_1)}{\sec \theta_1} \right\}. \quad (A-3)$$

Equation A-3 appears as Eq. 4 on page 6.

The solution to the equivalent volume cone approximation was designated FLUXM and the solution programmed was

$$\Phi(a) = \frac{S_V}{2\mu_s} \left\{ E_2(b_1) - \frac{E_2(b_1 \sec \theta_1)}{\sec \theta_1} - E_2(b_3) + \frac{E_2(b_3 \sec \theta_1)}{\sec \theta_1} \right\} \quad (A-4)$$

Equation A-4 appears on page 7 as Eq. 6.

The solution to the small cone approximation was designated FLUXS and the solution programmed was

$$\Phi(a) = \frac{S_V}{2\mu_s} \left\{ E_2(b_1) - \frac{E_2(b_1 \sec \theta_2)}{\sec \theta_2} - E_2(b_3) + \frac{E_2(b_3 \sec \theta_2)}{\sec \theta_2} \right\}. \quad (A-5)$$

Equation A-5 appears on page 6 as Eq. 5.

The solution to the equivalent circular plane source approximation was designated FLUXZ and the solutions programmed were

$$\Phi(a) = \frac{S_V h}{2} \left\{ E_1(b_2) - E_1(b_2 \sec \theta_z) \right\}, \text{ if } \mu_s h \leq 1.5 \quad (A-6)$$

and

$$\Phi(a) = \frac{S_V(1.5)}{2\mu_s} \left\{ E_1(b_2) - E_1(b_2 \sec \theta_z) \right\} \text{ if } \mu_s h > 1.5. \quad (A-7)$$

This was a trial and error solution where \underline{z} was altered as necessary to cause FLUXZ to approximate FLUX within a specified accuracy. Equations A-6 and A-7 appear on page 7 as Eqs. 7 and 8 with \underline{k} set at 1.5.

The program subrouting for $E_1(x)$ used different solutions for values of $\underline{x} < 1$ and for $\underline{x} \geq 1$.

For $\underline{x} < 1$

$$E_1(x) = -0.57721566 - \ln x + x - \frac{x^2}{4} + \frac{x^3}{18} - \dots \quad (A-8)$$

For $\underline{x} \geq 1$

$$E_1(x) = \frac{e^{-x}}{x} \left\{ \frac{a_0 + a_1 x + a_2 x^2 + a_3 x^3 + x^4}{b_0 + b_1 x + b_2 x^2 + b_3 x^3 + x^4} \right\} \quad (A-9)$$

where

$$a_0 = 0.26777373$$

$$b_0 = 3.9584969$$

$$a_1 = 8.6347609$$

$$b_1 = 21.099653$$

$$a_2 = 18.059017$$

$$b_2 = 25.632956$$

$$a_3 = 8.5733287$$

$$b_3 = 9.5733223$$

Equation A-8 is an infinite series and the choice of number of terms used was set by requiring that the ratio of the absolute value of the last term to the complete series be less than some specified value. Equation A-9 is an approximate solution developed by Hastings (5), accurate to within the limitations of the computer.

Input and output data associated with this program are listed in Tables A-1 and A-2 respectively.

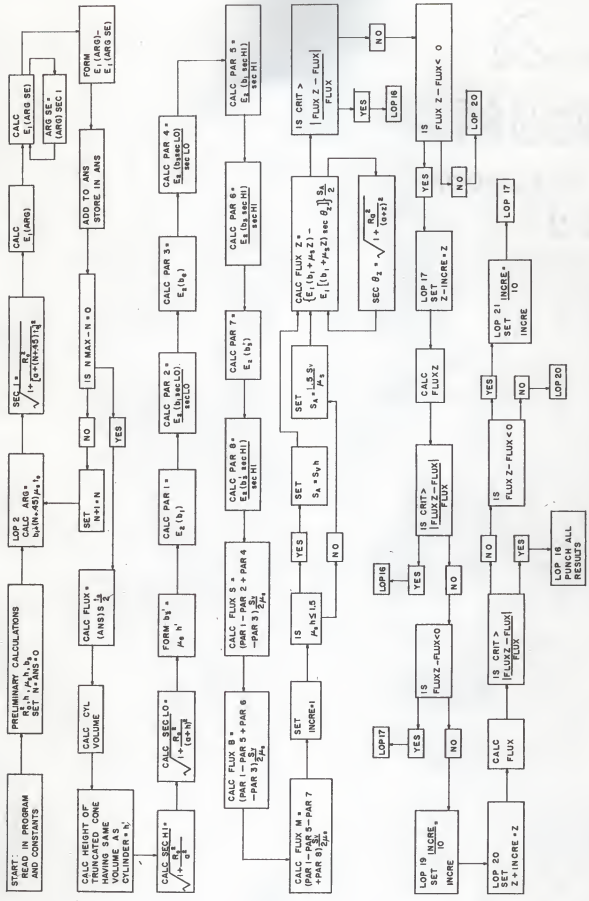
Table A-1. Input data required for use of the IBM 650 Computer program which calculates the centerline uncollided flux from the end of a finite right-circular cylinder.

Symbol	Explanation	Drum Storage Location
NMAX	One less than the number of disks in the cylinder	0100
TZRO	Disk thickness (cm)	0101
MUS	Cylinder cross section (cm^{-1})	0102
BONE	Shield mean free paths	0103
A	Shield thickness (cm)	0104
R	Cylinder radius (cm)	0105
S	Source strength ($\text{cm}^{-3} \text{sec}^{-1}$)	0106
CHK	Check to calculate or pass by a given cylinder	0107
ZZRO	Initial self-absorption values (cm)	0108
CRIT	Required precision of equivalent source flux calculation	0500
CRIT1	Cylinder height (mean free paths) for constant equivalent source strength	0550
PT45	Ratio of δ to disk thickness	0350

Table A-2. Identification table for print outs for centerline uncollided flux calculation from the end of a finite cylinder.

Card	Word	Symbol and/or Explanation
1	1	FLUX
	2	FLUXB
	3	FLUXM
	4	FLUXS
	5	FLUXZ
	6	z Self-absorption distance (cm)
	7	$(FLUX - FLUXZ) / FLUX$
	8	$\mu_s z$ Self-absorption distance mean free paths
2	1	FLUXB - FLUX
	2	$(FLUXB - FLUX) / FLUX$
	3	FLUXM - FLUX
	4	$(FLUXM - FLUX) / FLUX$
	5	FLUX - FLUXS
	6	$(FLUX - FLUXS) / FLUX$
3	1	HITE Cylinder height (cm)
	2	NMAX
	3	TZRO
	4	MUS
	5	BONE
	6	A
	7	R
	8	S
4	1	HITE+ A
	2	$(HITE) (MUS)$ Cylinder height mean free paths
	3	$(TZRO) (MUS)$ Disk thickness mean free paths
	4	$(R) (MUS)$ Radial mean free paths
	5	MU Shield cross section (cm^{-1})
	6	A + R
	7	A/R
	8	A/HITE

Approximate running time for the program is 5 minutes for NMAX equal to 100. The program is faster when $b_1 > 1$ due to the difference in the series calculations to be made.



LOGIC DIAGRAM APPENDIX A

	FOY 4		116	0154	34	0104	0204
	FAO 0WE		117	0204	12	0030	0277
	STU SECH1	SOROT	118	0527	69	0280	0283
	RAU WITE		119	0280	21	0284	0287
	FAO 4		120	0287	60	0006	0261
	STU HPR2		121	0281	31	0136	0239
	FMP 8003		123	0289	39	0003	0143
	STU HPR28		124	0143	60	0018	0103
	RAU 8900		125	0301	60	0018	0103
	FOY HPR28		126	0103	14	0146	0198
	FAO 0RE		127	0198	32	0050	0577
	LOO		128	0577	69	0130	0083
	STU SECL0	SOROT	129	0310	21	0334	0337
	RAU 80ME		130	0337	60	0103	0117
	LOO		131	0157	69	0060	0063
	STU PAR1	ET80	132	0060	21	0014	0067
	RAU 80ME		133	0067	60	0103	0267
	FMP SECL0		134	0207	39	0334	0384
	STU ASC1		135	0384	21	0088	0081
	FBR FP100		136	0091	33	0400	0627
	RAU		137	0627	46	0380	0331
	RAU ASC1	LOP6	138	0380	60	0088	0193
	LOO		139	0193	69	0146	0063
	FOY SECL0	ETW0	140	0146	34	0234	0434
	STU PAR8	LOP7	141	0434	21	0138	0141
LOP6	LOO ZRO		142	0331	69	0000	0203
	STO PAR2	LOP7	143	0203	24	0138	0141
LOP7	LOO		144	0141	60	0034	0289
	RAU 8THRE	ETW0	145	0289	69	0098	0063
	STU PAR3		146	0098	21	0194	0099
	RAU 8THRE		147	0099	60	0034	0239
	FMP SECL0		148	0339	39	0334	0404
	STU ASC2		149	0484	49	0484	0484
	FBR FP100		150	0191	33	0400	0677
	SWI		151	0677	46	0430	0381
	RAU ASC2		152	0430	60	0188	0243
	LOO		153	0243	69	0246	0063
	FOY SECL0	ET80	154	0249	24	0334	0534
LOP8	STU PAR4	LOP9	155	0534	21	0238	0241
	RAU 80ME		156	0241	69	0000	0283
LOP9	STU PAR4	LOP9	157	0283	21	0238	0241
	RAU 80ME		158	0241	60	0103	0287
	FMP SECH1		159	0287	39	0284	0584
	STU ASC3		160	0584	21	0288	0291
	FBR FP100		161	0291	33	0400	0727
	SWI		162	0727	46	0480	0431
	RAU ASC3	LOP10	163	0480	60	0380	0634
	LOO		164	0293	69	0296	0063
	FOY SECH1	ETW0	165	0063	34	0284	0634
LOP10	STU PAR5	LOP11	166	0634	21	0338	0341
	LOO ZRO		167	0431	69	0000	0303
	STO PAR5	LOP11	168	0303	24	0338	0341
LOP11	RAU 8THRE		169	0341	60	0034	0389
	FMP SECL0		170	0389	39	0284	0634
	STU ASC4		171	0684	21	0388	0391
	FBR FP100		172	0391	33	0400	0777
	SWI		173	0777	46	0530	0481
	RAU ASC4	LOP12	174	0481	60	0388	0343
	LOO		175	0343	69	0346	0063
	FOY SECH1		176	0346	34	0284	0734
	STU PAR6	LOP13	177	0734	21	0438	0441
LOP12	LOO ZRO		178	0441	69	0000	0353
	STO PAR6	LOP13	179	0353	24	0438	0441
LOP13	RAU 83PRM		180	0441	60	0234	0439
	LOO		181	0439	69	0148	0063
	STU PAR7		182	0142	21	0394	0149
	RAU 83PRM		183	0149	60	0234	0489
	FMP SECH1		184	0489	39	0284	0784
	STU ASC5		185	0784	21	0488	0491
	FBR FP100		186	0491	33	0400	0837
	SWI		187	0837	46	0580	0531
	RAU ASC5	LOP14	188	0580	60	0488	0393
	LOO		189	0393	69	0446	0063
	FOY SECH1	ETW0	190	0063	34	0484	0634
LOP14	STU PAR8	LOP15	191	0634	21	0538	0541
	LOO ZRO		192	0541	69	0000	0403
	STO PAR8		193	0403	24	0538	0541
LOP15	RAU PAR1		194	0541	60	0014	0039
	FBR PAR2		195	0039	33	0138	0165
	FAO PAR4		196	0165	32	0238	0215
	STU PAR3		197	0215	33	0296	0173
	STU ASC6		198	0173	21	0028	0581
	RAU 8		199	0581	60	0104	0511
	FOY HUB		200	0511	34	0104	0802
	FOY T80		201	0202	34	0150	0900
	STU ASC7		202	0900	21	0284	0307
	FMP ASC6		203	0307	39	0028	0078
	STU FLUX8		204	0078	60	0078	0083
	RAU PAR1	SMALL CORE	205	0083	60	0014	0069
	FBR PAR5		206	0069	33	0338	0283
	STU PAR9		207	0283	21	0020	0283
	FAO PAR6		208	0283	32	0438	0315
	STU PAR3		209	0315	33	0196	0373
	FMP ASC7		210	0373	39	0254	0304
	STU FLUX8	BIG CORE	211	0304	21	0006	0361
	RAU PAR9		212	0361	60	0020	0075
	FBR PAR7		213	0075	33	0396	0383
	FAO PAR8		214	0383	32	0538	0365
	FMP ASC7		215	0365	39	0254	0354
	STU FLUX8		216	0354	21	0038	0411
	LOO ZRO	WEO CORE	217	0411	69	0108	0441
	STO Z		218	0441	24	0064	0117
	LOO 0RE		219	0117	69	0050	0453
	STU ICRCE		220	0453	60	0434	0359
	RAU CFWFP		221	0359	60	0056	0511
	FBR CRIT1		222	0511	33	0580	0879
	SWI		223	0879	46	0630	0631
	RAU 8	LOP50	224	0630	60	0104	0261
	FMP WITE		225	0261	39	0006	0456
	FOY T80		226	0456	34	0150	0950
LOP50	STU ASC8	LOP51	227	0950	21	0404	0377
	RAU CRIT1		228	0377	60	0500	0185
	FOY HUB		229	0185	34	0150	0357
	FMP 8		230	0357	39	0108	0506
	FOY T80		231	0506	34	0150	1050
	STU ASC8	LOP51	232	1050	21	0404	0377
LOP51	RAU Z	CALC	233	0377	60	0064	0119
	LOO I	LOP20	234	0119	69	0078	0165
	STU ICRCE		235	0078	46	0175	0029
LOP17	RAU Z		236	0029	32	0175	0064
	FBR ICRCE		237	0165	33	0406	0183
	STU Z		238	0183	21	0064	0167
	LOO		239	0167	69	0070	0183
	RAU 8		240	0070	46	0175	0094
	SWI ICRCE	LOP19	241	0094	60	0406	0811
LOP19	FOY TER		242	0811	34	0300	1100
	STU ICRCE		243	1100	21	0406	0169
	RAU Z	LOP20	244	0169	60	0064	0219
LOP20	FAO ICRCE		245	0219	32	0406	0233

	FMP ARGUM	PRDCE	008 376	0543	39 0178 0228
	STU ARGUM		009 377	0228	21 0178 0493
PRDCE	LDD P000		010 378	0493	39 0148 0593
	STU U	CONT4	011 379	0637	24 0148 0593
	RAU ARGUM		012 380	0593	60 0178 0637
CONT4	FOV U		013 381	0637	34 0140 0190
	FDV U		014 382	0190	34 0140 0240
	FSE U		015 383	0240	33 0140 0317
	FDV THREE		016 384	0317	34 0240 0440
	STU CHECK		017 385	0440	21 0604 0557
	FOV U		018 386	0557	34 0140 0890
RAW R003			019 387	0890	47 8003 0077
RAW R005			020 388	0077	60 8003 0355
FSE P007			021 389	0355	13 0000 0385
RAW TEMP	CONT3		022 390	0385	46 0686 0739
RAW CHECK			023 391	0739	60 0604 0809
STU U	CONT4		024 392	0809	32 0140 0367
FAU U			025 393	0367	21 0148 0593
RAW CHECK			026 394	0604	60 0604 0859
FAU U			027 395	0859	32 0140 0437
FMP TEMP			028 396	0437	39 0000 0340
LDD R003	TEMPA		029 397	0340	69 8003 0213
RAW R004			030 398	1184	10 0000 0044
THREE	0051		031 399	0200	30 0000 0051
PRECT	0044		032 400	0208	10 0000 0044
LWX51	STO LMX08	EXIT INTRN	401 1450	24 0903 1006	
	NZE	LNX14	402 1006	45 0110 0961	
	RAW LNX14		403 0110	46 0961 0114	
	STU LMX09		404 0114	21 0168 0071	
	RSL FP006		405 0071	66 1184 0769	
	STU LMX10		406 0769	24 0192 0145	
	STL LMX09		407 0145	30 0549 0432	
	RAW LMX09		408 0432	60 0168 0593	
	STL LMX05		409 0593	30 1327 0800	
	STL LMX11		410 0900	20 0435 0738	
	L1L 0000		411 0738	35 0000 0607	
	FMP FIFTY	LNX04	412 0607	11 0160 0515	
	NZE	LNX04	413 0515	45 0118 0319	
	RAW LMX09	LNX05	414 0118	66 1184 0769	
	H80	R003	415 0121	61 8003 0289	
	LDD FP006		416 0289	49 1184 0607	
	STO LMX02	LNX03	417 0607	24 0249 0128	
	L1L 0000		418 0128	30 0000 0243	
	SCT 0000		419 0741	36 0000 0243	
	AUP SIXTY		420 0243	10 0066 0311	
	FMP R006		421 0171	11 8008 0279	
	RAW R003		422 0279	60 8003 0737	
	RAW R005		423 0737	39 0449 0899	
	FMP LATER	LNX04	424 0899	39 0509 0558	
	FMP LMX02		425 0558	61 1327 0800	
	RAL LMX09	LNX04	426 0139	65 0168 0757	
	R004		427 0757	30 8008 0389	
	RAW R002		428 0389	60 8008 0787	
	ALD FIFTY		429 0787	15 0168 0565	
	L1L 0000		430 0565	35 0009 0281	
	FAU FP006		431 0281	32 1184 1011	
	STU LMX09		432 1011	21 0168 0871	
	F30 FPTW0		433 0271	33 0128 0351	
	FOV LMX09		434 0351	14 0566 0368	
	STU LMX13		435 0566	21 0172 0225	
	STO LMX13		436 0225	26 0000 0113	
	STO LMX11		437 1131	24 0435 0788	
	FMP R001	LNX06	438 0788	39 8001 0791	
	STU FACTA		439 0791	21 0544 0349	
	RAW LMX10		440 0349	60 0192 0147	
	FAU FPTW0		441 0147	28 1184 0401	
	STU LMX10		442 0401	21 0192 0195	
	FMP FACTN		443 0195	60 0178 1377	
	FOV LMX10		444 1377	39 0546 0596	
	STU LMX13		445 0596	34 0192 0248	
	FAU LMX12		446 0248	21 0178 0275	
	FOV LMX13		447 0275	28 0277 0405	
	FBN R002		448 0405	21 0278 1181	
	FBN R001		449 1181	33 0435 1061	
	RAW R003		450 1061	34 1178 0485	
	FBN RIZE7		451 0485	67 8003 0643	
	LDD LMX12		452 0643	60 8008 0451	
	STU LMX12		453 0451	33 0654 1231	
	STU LMX13		454 1231	46 1234 0535	
	FMP LMX10	LNX06	455 0535	69 0278 1281	
	RAW LMX10		456 1281	24 0435 0830	
	STU LMX13		457 0830	60 0172 1427	
	FMP LMX10		458 1427	39 0192 0298	
	RAW LMX12		459 0298	21 0172 0349	
	STU LMX13		460 1234	60 0278 0603	
	FMP FPTW0		461 0603	27 0172 0174	
	F30 LMX05	LNX08	462 0174	33 1327 0803	
	R004		463 0803	41 0000 0174	
	FFTR0	0051	464 0184	20 0000 0051	
	RIZE7	0844	465 0844	60 0654 0654	
	INTEN	5151	466 0509	33 0258 5151	
	FIFTY	0000	467 0666	20 0000 0000	
	010 FIFTY	0060	468 0066	00 0000 0000	
	LWX14	0789	469 0961	01 0345 0789	
	ETOR	NALT	470 1000	24 0653 1056	
		EXIT INTRN	471 1056	21 0210 0313	
		STONE ANG	472 0313	21 0000 0313	
		ZERO	473 0321	37 0210 0837	
			474 0837	21 0345 0845	
			475 0845	69 0548 0501	
		ONE	476 0501	24 0790 0657	
		COEFF	477 0657	60 0342 0197	
		FIVE	478 0197	33 1550 1477	
			479 1477	26 1030 1321	
			480 1331	81 0342 0295	
			481 0295	60 0790 0909	
		E TO 5	482 0909	39 0512 0152	
			483 0152	33 0453	
			484 1030	60 0342 0247	
			485 0247	33 0248 0385	
		ONE	486 0385	46 0328 0379	
			487 0379	21 0348 0385	
			488 0345	60 0704 0959	
		E TO 1	489 0959	39 0212 0262	
			490 0262	21 0704 1030	
			491 0328	60 0342 0297	
		POINT TWO	492 0297	33 1600 1837	
			493 1527	46 1080 1361	
			494 1361	21 0348 0395	
			495 0395	60 0704 1099	
		E TO PT 8	496 1099	39 0312 0368	
			497 0368	29 0000 0388	
			498 1080	60 0342 0347	
			499 0347	29 1600 0903	
			500 1600	39 0704 0754	
			501 0754	01 0258 1111	
			502 1111	20 0000 0615	
			503 0615	46 0312 0369	
			504 0369	60 0258 0853	
			505 0853	60 0248 0953	

STU	EEE3						
RAU	EEE2						
FAD	CCC3						
FMP	EEE5						
FAD	CCC2						
FMP	EEE2						
FAO	CCC1						
FMP	EEE2						
FAD	CCC0						
FDV	EEE3						
FDV	EEE2						
STU	EEE4						
RBU	EEE2						
LDD							
FMP	EEE4	ETOX					
R6	7773	EE1					
CCC0	86	7350					
CCC1	86	3476					
CCC2	18	0951					
CCC3	85	1752					
ODD0	39	7332					
ODD1	39	8842					
ODD2	21	0996					
ODD3	25	3352					
	35	3329					
	93	7332					
		8652					
		2551					

DENUMNATOR	636	0735	21	0390	0693	
	637	0693	60	1354	1411	
	638	1411	32	0264	1091	
	639	1091	19	1354	1356	
	640	1556	32	1459	0785	
	641	0785	39	1354	1406	
	642	1406	32	1509	0835	
	643	0835	39	1354	1856	
	644	1606	32	1559	0885	
	645	0885	34	0390	0440	
RATID	646	0440	14	1354	1756	
ALLBUTETDX	647	1756	21	0966	0463	
	648	0463	61	1354	1461	
	649	1461	69	0314	1500	
EDONEOFEE2	650	0314	39	0260	0348	
	651	1509	26	7773	7350	
	652	1509	86	3476	0951	
	653	1459	18	0962	1752	
	654	0264	85	7332	8751	
	655	1409	39	5649	6951	
	656	1359	21	0996	5352	
	657	1309	25	3329	3652	
	658	0214	95	7332	3351	

APPENDIX B

Description of IEM 650 Computer Program
Used to Calculate the Error in Centerline Uncollided Flux
Determination from the End of a Finite Right-circular Cylinder
by the Use of an Equivalent Circular Plane Source

This program was written to calculate the error of a flux determination by the empirical method developed in this thesis. The program was written in Soap II computer language using floating point operations. The logic diagram and the object program are given in this appendix.

The solution to the equivalent circular plane source approximation was designated ABC9 and the solutions programmed were

$$\Phi(a) = \frac{S_V}{2} \left\{ E_1(b_2) - E_1(b_2 \sec \theta_z) \right\}, \quad \text{if } \mu_s h \leq 1.5; \quad (\text{B-1})$$

$$\Phi(a) = \frac{S_V(1.5)}{2\mu_s} \left\{ E_1(b_2) - E_1(b_2 \sec \theta_z) \right\}, \quad \text{if } \mu_s h > 1.5. \quad (\text{B-2})$$

Equations (B-1) and (B-2) appear as Eqs. A-6 and A-7 in Appendix A. The program subroutine for $E_1(x)$ is identical to that described in Appendix A.

Input data and output data associated with this program are listed in Tables B-1 and B-2 respectively.

Table B-1. Input data required for use of the IBM 650 Computer program which calculates the error in the empirical solution of the centerline uncollided flux from the end of a finite right-circular cylinder.

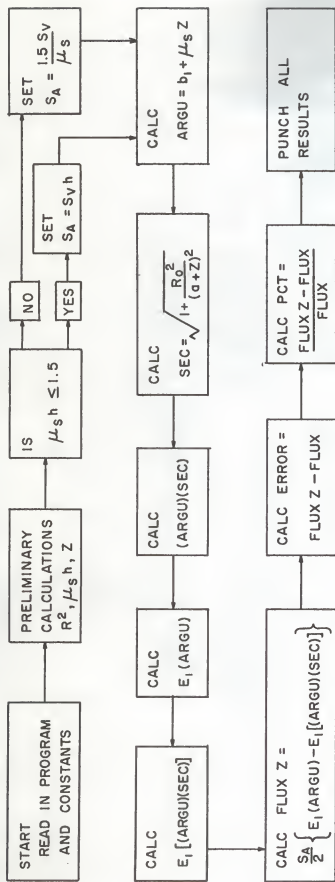
Symbol	Explanation	Drum Storage Location
HITE	Cylinder height (cm)	0000
BONE	Shield mean free paths	0001
FLUX	Actual flux ($\text{cm}^{-2} \text{sec}^{-1}$)	0003
S	Source strength ($\text{cm}^{-3} \text{sec}^{-1}$)	0004

Table B-1. (concl)

Symbol	Explanation	Drum Storage Location
R	Cylinder radius (cm)	0005
A	Shield thickness (cm)	0006
MUS	Source cross section (cm^{-1})	0008
MUSZ	Empirically determined self-absorption distance (mean free paths)	0009

Table B-2. Identification table for print outs for error calculation.

Card	Word	Symbol and/or Explanation
1	1	FLUX accurate flux solution
	2	ABC9 approximate flux solution
	3	ERROR ABC9 - FLUX
	4	PCT (ABC9 - FLUX)/FLUX
	5	z self-absorption distance
	6	A
	7	R
	8	BONE
2	1	HITE
	2	MUS
	3	$\mu_0 h$ Cylinder height (mean free paths)
	4	$\bar{\mu}$ Shield cross section
	5	MUSZ
	6	MUSZ + BONE
	7	A + R
	8	A/R



LOGIC DIAGRAM APPENDIX B

OBJECT PROGRAM FOR CALCULATION OF ERROR IN EQUIVALENT CIRCULAR PLANE SOURCE FLUX DETERMINATION

```

HLR 1951      1960      1      0000      00 0000 0000      -0000000000000000
HLR 1977      1984      2      0000      00 0000 0000      -0000000000-00000
BLW 1700      1749      3      0000      00 0000 0000      -0000000000-00000
SVN HITE      0000      4      0000      00 0000 0000      -0000000000-00000
SVN DOME      0001      5      0000      00 0000 0000      -0000000000-00000
SVN FLUX      0003      6      0000      00 0000 0000      -0000000000-00000
SVN SARC      0004      7      0000      00 0000 0000      -0000000000-00000
SVN R         0005      8      0000      00 0000 0000      -0000000000-00000
SVN A         0006      9      0000      00 0000 0000      -0000000000-00000
SVN WUS2      0008      10     0000      00 0000 0000      -0000000000-00000
SVN WUS2      0009      11     0000      00 0000 0000      -0000000000-00000
SVN START     1000      12     0000      00 0000 0000      -0000000000-00000
FP100        10 0000      0053      HUNOREU      13 019R      10 0000 L053
ONE          10 0000      0051      ONE          14 0100      10 0000 0051
TWO          10 0000      0051      ONE          15 0150      20 0000 0051
CRIT1        15 0000      0051      ONE          16 0200      15 0000 0051
RAU ROME1    LOP1      LOP1      17 1000      60 0001 0055
FBR 1700     LOP1      EOCL      18 0050      33 1700 0057
WZ          LOP1      EOCL      19 0057      45 0030 0031
LD          LOP1      EOCL      20 0030      69 0033 0036
PCR 1977     LOP1      EOCL      21 0053      71 1977 0077
PCM 1977     LOP1      EOCL      22 0077      71 1977 0147
PCH 1977     LOP1      EOCL      23 0127      71 1977 0030
RAU R        LOP1      EOCL      24 0011      60 0005 0049
FMP R003     LOP1      EOCL      25 0059      39 8003 0013
STU S900     LOP1      EOCL      26 0013      60 0018 0051
RAU WUS2     LOP1      EOCL      27 0021      60 0009 0063
FVU WUS      LOP1      EOCL      28 0003      34 0008 0058
STU Z        LOP1      EOCL      29 0058      21 0018 0015
RAD HITE     LOP1      EOCL      30 0015      60 0000 0105
FMP WUS      LOP1      EOCL      31 0105      39 0006 0108
FBR CRIT1    LOP1      EOCL      32 0108      33 0200 0177
HWI          LOP1      EOCL      33 0177      46 0006 0081
RAU S        LOP1      EOCL      34 0080      60 0004 0109
FAD HITE     LOP1      EOCL      35 0109      39 0000 0250
FVU TEO      LOP1      EOCL      36 0250      34 0150 0300
STU ABC0     LOP1      EOCL      37 0300      21 0054 0007
RAU CRIT1    LOP2      EOCL      38 0001      30 0200 0152
FVU WUS      LOP2      EOCL      39 0155      34 0008 0158
FMP S        LOP2      EOCL      40 0158      39 0004 0104
FVU TEO      LOP2      EOCL      41 0104      34 0150 0350
STU ARC0     LOP2      EOCL      42 0350      21 0054 0007
RAU Z        LOP2      EOCL      43 0007      60 0012 0017
LD          LOP2      EOCL      44 0017      69 0020 0023
LDU FLOX     LOP2      EOCL      45 0000      60 0000 0066
HTD 1977     LOP2      EOCL      46 0056      24 1977 0130
LDU ARC9     LOP2      EOCL      47 0130      69 0003 0064
STU 1978     LOP2      EOCL      48 0086      24 1978 0111
LDU LER00R   LOP2      EOCL      49 0111      69 0034 0037
STU 1979     LOP2      EOCL      50 0037      24 1979 0038
LDU PCT      LOP2      EOCL      51 0038      69 0035 0038
STU 1980     LOP2      EOCL      52 0038      24 1980 0133
LDU Z        LOP2      EOCL      53 0133      69 0012 0065
STU 1981     LOP2      EOCL      54 0065      24 1981 0085
LDU A        LOP2      EOCL      55 0084      69 0006 0109
STU 1982     LOP2      EOCL      56 0109      24 1982 0085
LDU R        LOP2      EOCL      57 0085      69 0005 0058
STU 1983     LOP2      EOCL      58 0088      24 1983 0136
LDU ROME     LOP2      EOCL      59 0136      69 0001 0154
STU 1984     LOP2      EOCL      60 0154      24 1984 0087
STU 1700     LOP2      EOCL      61 0087      24 1700 0053
PCH 1977     LOP2      EOCL      62 0053      71 1977 0227
RAU HITE     LOP2      EOCL      63 0227      60 0004 0005
STU 1977     LOP2      EOCL      64 0005      21 1977 0180
FMP WUS      LOP2      EOCL      65 0180      39 0006 0258
STU 1978     LOP2      EOCL      66 0258      24 1978 0181
STU 1979     LOP2      EOCL      67 0181      21 1979 0089
RAU ROME     LOP2      EOCL      68 0089      60 0001 0255
FVU A        LOP2      EOCL      69 0255      34 0006 0106
STU 1980     LOP2      EOCL      70 0106      24 1981 0134
LDU WUS2     LOP2      EOCL      71 0133      69 0009 0062
STU 1981     LOP2      EOCL      72 0062      24 1981 0134
LDU ARCO     LOP2      EOCL      73 0134      69 0137 0040
STU 1982     LOP2      EOCL      74 0040      24 1982 0135
RAU A        LOP2      EOCL      75 0135      60 0006 0011
FAD R        LOP2      EOCL      76 0011      32 0005 0231
STU 1983     LOP2      EOCL      77 0231      21 1983 0186
RAU R        LOP2      EOCL      78 0186      60 0005 0209
FMP WUS      LOP2      EOCL      79 0209      60 0000 0308
STU 1984     LOP2      EOCL      80 0308      21 1984 0187
PCH 1977     LOP2      EOCL      81 0187      71 1977 0277
LD          LOP2      EOCL      82 0277      69 0230 0036
FMP 1977     LOP2      EOCL      83 0230      71 1977 8000
STU CALL     LOP2      EOCL      84 0033      24 0026 0029
FVU WUS      LOP2      EOCL      85 0029      39 0009 0358
FAD ROME     LOP2      EOCL      86 0358      34 0001 0327
STU ARCU     LOP2      EOCL      87 0327      21 0137 0090
LD          LOP2      EOCL      88 0090      69 0003 0066
STU EONE1    LOP2      EOCL      89 0043      21 0048 0051
RAU A        LOP2      EOCL      90 0051      60 0006 0061
FAD Z        LOP2      EOCL      91 0061      32 0012 0339
FMP R003     LOP2      EOCL      92 0039      39 8003 0093
STU HTS00    LOP2      EOCL      93 0093      21 0098 0101
RAU MSUD     LOP2      EOCL      94 0101      60 0018 0073
LDU HTS00    LOP2      EOCL      95 0073      34 0000 0148
FAU UNE      LOP2      EOCL      96 0148      32 0100 0377
LDU HTS00    LOP2      EOCL      97 0377      69 0280 0233
FMP ARC0     LOP2      EOCL      98 0280      39 0000 0245
STU ARC15    LOP2      EOCL      99 0245      21 0042 0045
FBR FP100    LOP2      EOCL      100 0045      33 0198 0025
RAU ARC15    LOP2      EOCL      101 0025      46 0028 0079
LD          LOP2      EOCL      102 0028      60 0002 0047
HTU CONE2    LOP2      EOCL      103 0047      69 0400 0046
LDU ZNO      LOP2      EOCL      104 0000      21 0400 0057
LDU ZNO      LOP2      EOCL      105 0079      69 0050 0103
STU ZNO      LOP2      EOCL      106 0103      24 0204 0057
FMP ARC0     LOP2      EOCL      107 0057      60 0000 0153
FBR ROME     LOP2      EOCL      108 0153      33 0204 0201
STU ARCU     LOP2      EOCL      109 0201      39 0014 0034
STU ARCU     LOP2      EOCL      110 0554      21 0003 0036
STU FLUX     LOP2      EOCL      111 0236      33 0003 0129
STU LER00R   LOP2      EOCL      112 0129      21 0034 0087
FVU FLUX     LOP2      EOCL      113 0087      34 0003 0209
STU PCT      LOP2      EOCL      114 0209      21 0015 0026
ONE          10 0000      0051      ONE          115 0100      10 0000 0051

```


	FUP LNTEH	LNx04	246	0339	39	0542	0592
	STH LNKO0		247	0592	21	0677	0119
LNx04	RAL LNKO0		248	0119	63	0118	0173
	BRT 0000		249	0173	30	0009	0379
	ALN FFF02		250	0379	60	0006	0437
	SLT 0000		251	0437	15	0110	0215
	FST FFOHE		252	0215	35	0002	0321
	STO LNKO9		253	0321	32	0174	0401
	FST FFOHE		254	0401	31	0118	0371
	STO LNKO9		255	0371	31	0118	0263
	FST FFOHE		256	0263	34	0118	0216
	STO LNKO9		257	0216	21	0075	0473
	FST FFOHE		258	0175	24	0129	0481
	STO LNKO9		259	0481	24	0129	0136
	FST FFOHE		260	0136	39	0001	0141
	STO LNKO9		261	0141	41	0146	0149
LNx06	STO LNKO6	LNx06	262	0149	60	0181	0487
	FAO FFOHO		263	0487	32	0336	0113
	STU LNKO0		264	0113	21	0189	0335
	RAD LNKO3		265	0335	60	0072	0777
	FMP FAKT8		266	0777	39	0246	0826
	FOV LNKO10		267	0296	34	0182	0232
	FST LNKO1		268	0232	21	0126	0531
	FAO LNKO2		269	0531	33	0085	0211
	STO LNKO2		270	0211	34	0085	0385
	FBN LNKO11		271	0385	77	0003	0243
	FOV LNKO11		272	0243	60	0004	0451
	RAW ROO3		273	0451	33	0484	0581
	RAO ROO2		274	0243	60	0004	0451
	FST LNKO7		275	0581	46	0234	0435
	HMI LNKO7		276	0435	69	0128	0631
	STO LNKO11		277	0631	24	0085	0188
	FST LNKO11		278	0188	60	0072	0827
	RAW LNKO3		279	0827	39	0182	0282
	FMP LNKO10		280	0282	21	0072	0149
LNx07	STU LNKO3	LNx06	281	0282	60	0128	0483
	RAW LNKO3		282	0234	60	0128	0483
	FMP FFOHO		283	0403	39	0336	0536
	FST LNKO6		284	0536	31	0077	0513
	LN 0000	LNx06	285	0174	10	0000	0051
FFONE	FF FFOH		286	0336	10	0000	0051
	SIZE7		287	0454	10	0000	0044
	LN 0000	CRITERIA	288	0548	23	0258	1511
	LN 25 0850		289	0859	11	0000	0000
	FF FFOH		290	0066	00	0000	0060
	SIZE7		291	0161	01	2143	1769
	LN 0000	HALT	292	0446	24	0199	0000
	STO EEE1	FRIT INSTR	293	0002	23	0306	0539
	FBN ONE	ARGUMENT	294	0539	33	0100	0877
EOHES	RAW ONE8	EOHES	295	0877	46	0506	0681
	RAW FEER	SMALL ARG	296	0506	60	0506	0261
	LN 0000	LN FEER	297	0261	60	0084	0700
	LN FEES	LN FEER	298	0084	21	0568	0421
	RRN FFE13	GAMMA	299	0421	61	0224	0459
	FBN FFE15		300	0459	23	0368	0455
	FAO FFE12		301	0495	32	0508	0533
	STU FFE12	PARTIALARG	302	0533	02	0236	0121
	RAW FFO		303	0191	60	0150	0400
	STO FFE9	N	304	0405	24	0456	0311
	FMP ROO3		305	0311	39	0003	0265
	STO FFE10	DENOM	306	0265	21	0070	0223
	LN 0000		307	0223	69	0506	0609
	STO FEEB	NUM	308	0609	24	0412	0335
	RHO FFE12		309	0315	11	0106	0361
	FMP FFEH		310	0361	39	0412	0462
	STO FEEH	HUMPRATOR	311	0462	11	0412	0365
	FOV FFE10		312	0365	34	0070	0120
	HMI		313	0120	11	0074	0275
	FAO FFE12	NTM TENM	314	0277	32	0530	0415
	STU FFE12		315	0415	21	0238	0241
	FAO FFE11	TOTAL SOM	316	0241	60	0050	0455
	FAO FFE11		317	0455	37	0274	0501
	FAO FFE11		318	0501	34	0238	0288
	FBN FFE13		319	0288	33	0191	0067
	RAW FFE10		320	0067	46	0170	0471
	FAO FFE10	EEE14	321	0170	60	0230	0199
	STO FFE9	EEE1	322	0508	60	0070	0273
	FAO FFE9		323	0273	34	0458	0508
	RAW FFE10		324	0508	21	0070	0273
	RAO FFE9		325	0573	60	0458	0363
	FAO ONE		326	0363	32	0180	0977
	STU FFE9	NEW N	327	0977	81	0458	0411
	FMP ROO3		328	0411	39	0003	0465
	STO FFE10		329	0465	39	0074	0260
	FAO FFE10	EEF7	330	0260	21	0070	0315
EEE13	LN 0000	GAMMA	331	0264	17	0412	0411
EFF15	LN 0000	CRITFRIA	332	0221	10	0000	0044
CCC3	LN 0000	LRD	333	0300	00	0000	0000
ONE	LN 0000	ONE	334	0100	10	0000	0051
TBU	LN 0000	LARGE ARG	335	0100	35	0130	0011
CONEL	RAW EEE2		336	0601	60	0506	0481
	FAO ROO3		337	0481	32	0114	0341
	FMP FFE12		338	0341	39	0204	0566
	FAO ROO2		339	0269	32	0639	0485
	FMP FFE14		340	0485	39	0506	0606
	FAO ROO1		341	0606	38	0709	0535
	FMP FFE12		342	0535	39	0506	0606
	FAO OOOO		343	0606	32	0750	0585
	STH FFE12		344	0585	21	0194	0293
	FAO FFE12		345	0293	60	0506	0511
	FBN CCC3		346	0511	32	0164	0391
	FMP FFE12		347	0391	39	0506	0606
	FAO CCC2		348	0706	32	0809	0635
	FMP FFE14		349	0635	39	0506	0704
	FAO CCC1		350	0756	32	0939	0605
	FMP FFE12		351	0605	39	0506	0704
	FAO CCC0		352	0006	38	0909	0735
	FMP FFE13		353	0735	34	0190	0240
	FUV FFE14		354	0240	34	0506	0836
	STH EEE4		355	0836	21	0160	0433
	RAW LNKO3	ALLHHTETR	356	0433	31	0506	0561
	LN 0000	EEF1	357	0561	69	0214	0500
	LN 0000	FNOFPLLM	358	0114	39	0160	0199
	LN 0000		359	0909	36	0773	7350
	LN 0000		360	0199	66	0346	0951
	LN 0500		361	0109	11	0508	1752
	LN 7336		362	1752	25	7336	0751
	LN 0000		363	0739	39	5044	6951
	LN 0000		364	0709	21	0906	3362
	LN 0002		365	0639	85	6348	2652
	LN 7336		366	0114	95	7336	2351

UNCOLLIDED FLUX FROM FINITE
RIGHT-CIRCULAR CYLINDER
VIEWED ENDWISE

by

LARRY A. RASH

B. S., Kansas State University, 1957

AN ABSTRACT OF A THESIS

submitted in partial fulfillment of the

requirement for the degree

MASTER OF SCIENCE

Department of Nuclear Engineering

KANSAS STATE UNIVERSITY
Manhattan, Kansas

1962

An IBM 650 Computer code was written to solve for the flux from the end of a finite circular cylinder. This code was then used to solve for the flux from cylinders of varying size and absorption coefficient as well as for varying shield thickness and absorption coefficients.

From the information obtained, a method was developed to determine fluxes from cylinders by considering them to be replaced by a circular plane source. This circular plane source is located within the confines of the cylinder and has the same radius as the cylinder. This method makes it possible to determine the uncollided flux from the end of a cylinder more accurately than has previously been possible with only a desk calculator.

Curves and supporting information as necessary are presented to enable users to determine the source strength of the circular plane source and its location within the cylinder.